SUBUNIT COMPOSITION OF THE HUMAN CYTOPLASMIC DYNEIN-2 COMPLEX.

DAVID ASANTE[1,2], NICOLA L. STEVENSON[1], AND DAVID J. STEPHENS*

CELL BIOLOGY LABORATORIES, SCHOOL OF BIOCHEMISTRY, MEDICAL SCIENCES BUILDING, UNIVERSITY OF BRISTOL, BS8 1TD TEL: 00 44 117 331 2173

*CORRESPONDING AUTHOR. EMAIL: DAVID.STEPHENS@BRISTOL.AC.UK

[1] These authors contributed equally to this work.

[2] PRESENT ADDRESS: MAMMALIAN GENETICS UNIT, MRC HARWELL, HARWELL SCIENCE AND INNOVATION CAMPUS, OXFORDSHIRE OX11 0RD, UK.

KEYWORDS: MICROTUBULE MOTOR, DYNEIN, CILIA, INTRAFLAGELLAR TRANSPORT.

Number of words (not including references): 7608

SUMMARY

Cytoplasmic dynein-2 is the motor for retrograde intraflagellar transport and mutations in dynein-2 are known to cause skeletal ciliopathies. Here we define for the first time the composition of the human cytoplasmic dynein-2 complex. We show that the ciliopathy genes WDR34 and WDR60 are bona fide dynein-2 intermediate chains and are both required for dynein-2 function. In addition, we identify TCTEX1D2 as a unique dynein-2 light chain that is itself required for cilia function. We define several subunits common to both dynein-1 and dynein-2 including TCTEX-1 and -3, Roadblock-1 and -3, and LC8-1 and -2 light chains. We also find that NudCD3 associates with dynein-2 as it does with dynein-1. In contrast, the common dynein-1 regulators dynactin, LIS1, or BICD2 are not found in association with dynein-2. These data explain why mutations in either WDR34 or WDR60 cause disease as well as identifying TCTEX1D2 as a candidate ciliopathy gene.

INTRODUCTION

Normal cell function depends on the accurate movement and positioning of intracellular organelles and protein complexes. Microtubule motor proteins are critical to these processes, with the cytoplasmic dyneins being the primary minus-end directed microtubule motors. Two cytoplasmic dynein complexes exist in mammalian cells; dynein-1 is the better characterized of these, being involved in membrane traffic, organelle dynamics and chromosome segregation during mitosis (Paschal and Vallee, 1987). The cytoplasmic dynein-2 complex on the other hand, mediates the retrograde component of intraflagellar transport (IFT), the process by which primary and motile cilia as well as flagella function (Gibbons et al., 1994; Criswell et al., 1996). Retrograde IFT is essential for normal developmental signalling, notably the Hedgehog pathway in which dynein-2 acts in concert with the IFT-A particle to drive transport of activated components of this pathway from the cilia tip to the cell body (Huangfu and Anderson, 2005; Liu et al., 2005; May et al., 2005). Furthermore, IFT-A is known to be required for the loading of key components into cilia (Mukhopadhyay et al., 2010; Liem et al., 2012). Defects in the function of primary cilia lead to a cohort of human diseases known as the ciliopathies (Waters and Beales, 2011); among these, mutations in components of the dynein-2 complex cause Jeune syndrome, short rib polydactyly type III, and asphyxiating thoracic dystrophy (Dagoneau et al., 2009; Huber et al., 2013; McInerney-Leo et al., 2013; Schmidts et al., 2013b; Schmidts et al., 2013a).

Dynein-1 is comprised of a dimer of heavy chain subunits (encoded by the DYNC1H1 gene) which associate with two copies of an intermediate chain (DYNC1I1 or DYNC1I2 depending on the tissue type), two copies of one of two light intermediate chains (DYNC1LI1 or DYNC1LI2), and a number of light chain subunits (which includes the dynein light chain (DYNLL1), roadblock (DYNLRB1 and DYNLRB2), and Tctex families (DYNLT1, DYNLT3) (Pfister et al., 2005; Wickstead and Gull, 2007; Kardon and Vale, 2009)). The light chains are required for the correct assembly of the dynein complex and have been implicated in controlling its association with cargo molecules. For the majority of its functions, dynein-1 also associates with one or more binding partners (Kardon and Vale, 2009; Splinter et al., 2012). The best described of these are the dynactin complex, Lissencephaly-1 protein (LIS1), and bicaudal gene products (notably BICD2) (Splinter et al., 2012). In contrast, the molecular composition of the dynein-2 complex, notably in mammals, is not well defined.

Although specific genes encoding a dynein-2-specific heavy (DYNC2H1, also known as DHC1b and DHC2 (Criswell et al., 1996)) and light intermediate chains (DYNC2LI1 also known as LIC3 (Grissom et al., 2002)) have been identified, the full subunit composition of the motor and biochemical characterization of the subunit composition in metazoans is lacking. Model organisms such as *Chlamydomonas* and *Tetrahymena* have provided further clues that equivalents to the other known dynein-1 subunits are also present. *Chlamydomonas* genes encoding FAP133 and FAP163 (orthologues of mammalian WDR34 and WDR60 respectively) encode functional intermediate chains of algal dynein-2 (Rompolas et al., 2007; Patel-King et al., 2013). FAP133 was shown to have putative LC8 binding motifs and to localize around the basal body and within the flagellum (Rompolas et al., 2007). Furthermore, LC8 is known to play roles outside of the context of the dynein-1 complex which could explain some of the FAP133/WDR34 data to date. Our own work has shown that WDR34 localizes to the pericentrosomal region and is required for ciliogenesis and proper cilia function in vitro (Asante et al., 2013). We have also previously defined a role for the dynein light chain Tctex-1 in cilia length control, presumably in association with dynein-2 (Palmer et al., 2011). Others have also shown that WDR34 localizes to a pericentrosomal region and also that a fluorescent protein fusion of WDR34 (WDR34-tGFP) is present in cilia (Schmidts et al., 2013a). Furthermore WDR34-tGFP co-immunoprecipitated with FLAG-tagged LC8 consistent with a role for WDR34 in dynein-2 function.

FAP163 has also been shown to localize to the flagellar matrix, to co-purify with FAP133 and LC8, and, in the planarian *Schmidtea mediterranea*, to be absolutely required for ciliogenesis (Patel-King et al., 2013). Recent work from several groups has shown that mutations in the human orthologues of FAP133 (WDR34) and FAP163 (WDR60) cause skeletal ciliopathies (Huber et al., 2013; McInerney-Leo et al., 2013; Schmidts et al., 2013a). While these data are consistent with WDR34 and possibly WDR60 being key components of human dynein-2, biochemical data validating this are lacking. It also remains unclear whether dynein-2 works in cooperation with dynactin or other dynein-1 accessory complexes. LIS1, for example, is known to function in concert with both cytoplasmic dynein-1 (Faulkner et al., 2000) and the axonemal dyneins (Pedersen et al., 2007).

Since a metazoan dynein-2 complex has not been described in detail, we set out to define the subunit composition of the human dynein-2 complex and determine whether known dynein-1 regulators also modulate the function of this poorly characterized second cytoplasmic dynein motor.

RESULTS

We generated a human telomerase immortalized retinal pigment epithelial (hTERT-RPE1) cell line stably expressing WDR34 fused to a monomeric form of GFP (mGFP). Figure 1 shows that mGFP-WDR34 localizes to centrosomes and primary cilia in serum starved cells as well as showing a diffuse cytoplasmic distribution. This localization to cilia was confirmed by co-labelling with antibodies directed against acetylated tubulin (Fig. 1A). mGFP-WDR34 also colocalizes at the base of the cilium with known components of the basal body (γ-tubulin, ODF2, and OFD1, Fig. 1B-D). Fig. 1E shows that the localization of mGFP-WDR34 within cilia differs from that of the endogenous protein which localizes to pericentrosomal structures; Fig. 1F shows that the localization of mGFP-WDR34 to cilia is specific as GFP alone is not localized in cilia.

We sought to use this cell line to define the other proteins associated with WDR34. To achieve this we took a proteomic approach comparing the interactome of mGFP-WDR34 with mGFP using a GFP-nanotrap (Rothbauer et al., 2006). Supplementary Table 1 shows the proteomics data for all known dynein-1 and putative dynein-2 components that were identified in this experiment. Supplementary Table 1A shows the highly efficient isolation of mGFP-WDR34 using this approach. Large numbers of peptides and spectra were also seen for WDR60 as well as the known dynein-2 heavy chain (DYNC2H1). We also detected (albeit at low abundance) the known dynein-2 light intermediate chain subunit DYNC2LI1/LIC3. Listed in Supplementary Table 1B are the dynein light chains that we identified. Here, all known dynein-1 light chain isoforms (LC8-1 and -2, Tctex-1 and -3, and Roadblock-1 and -2) were identified in association with mGFP-WDR34. In addition we detected TCTEX1D2 (also known as Tctex-2). This subunit is not found in association with mGFP alone. We also noted (Supplementary Table 1C) the association of mGFP-WDR34 with two regulators of dynein-1 function NudC and NudCD3 (also called NudC-like or NUDCL). Supplementary Table 1D then shows the data for the key dynein accessory factors that were detected in our proteomics. These show that mGFP-WDR34 does not associate with dynactin, Bicaudal 1, or LIS1 (PAFAH1B) at levels above that of mGFP alone. Bicaudal 2, Spindly, NudE, and Nudel, all of which are known accessory factors for dynein-1, were not detected at all. We then used these proteomic data to guide our further biochemical analyses.

The above data indicate that both WDR34 and WDR60 are intermediate chains of the dynein-2 complex. These findings were then validated using immunoblotting. Fig. 2A shows specific isolation of mGFP-WDR34. Importantly we find that the endogenous WDR34 does not co-immunoprecipitate with mGFP-WDR34 suggesting that the recombinant form does not form a complex with the endogenous protein. Immunoblotting for WDR60 showed that this was highly efficiently isolated in complex with mGFP-WDR34 (Fig. 2B) implying that these two putative intermediate chains might be present in the same complex. As expected from the proteomic data, the canonical dynein-1 intermediate chain, IC74, was not immunoprecipitated with mGFP-WDR34 (Fig. 2C) nor was a negative control protein, GAPDH (Fig. 2D). Two components of the dynactin complex, $p150^{Glued}$ (Fig. 2E) and $p50^{dynamitin}$ (Fig. 2F) also failed to immunoprecipitate with mGFP-WDR34; similarly, LIS1 was not detected (Fig. 2G). In contrast Tctex-1 (Fig. 2H) and NudCD3 (Fig. 2I) were both efficiently isolated. Consistent with our identification of TCTEX1D2 in our proteomics, we were able to identify TCTEX1D2 in association with mGFP-WDR34 (Fig. 2J). TCTEX1D2 is not detectable in whole cell lysates but the enrichment following GFP-nanotrap isolation of mGFP-WDR34 enables its detection in immunoprecipitates (Fig. 2J). These data reveal some specificity since both Tctex-1 and NudCD3, but not TCTEX1D2, associate with dynein-1 as determined in five independent pull downs of dynein-1; dynactin, LIS1, and BICD2 were also always identified in these dynein-1 pull-downs from both HeLa and RPE-1 cells (unpublished observations). We have been unable to analyze the dynein-2 heavy chain or light intermediate chain subunits by immunoblotting owing to a lack of available antibodies.

Dynein-2 is predicted to be a large molecular weight complex with a high sedimentation coefficient, similar to cytoplasmic dynein-1. As predicted for a large macromolecular complex, we found endogenous WDR34 in a large complex that sedimented on sucrose density gradients in similar fractions to the dynein-1 intermediate chain (Fig. 3A). This suggests that WDR34 functions in the context of a high molecular weight complex. As expected, mGFP-WDR34 and WDR60 were both found in large complexes (Fig. 3B and C) consistent with their role as intermediate chains within the same dynein-2 complex. In contrast, mGFP (Fig. 3B), like the majority of the control protein GAPDH, was found predominantly in low density fractions as expected. GAPDH is known to associate with many other proteins including dynein-1 (Zala et al., 2013) which likely explains the low amounts detected across the higher density gradient fractions.

The expression of mGFP-WDR34 had no significant effect on the distribution of WDR60 across the complex (Fig. 3C). Some unincorporated mGFP-WDR34 was observed as well as some mGFP itself (Fig. 3C), most likely arising as a result of proteolytic processing of the recombinant protein at the linker site between mGFP and WDR34. This could also explain much of the diffuse cytoplasmic labelling seen in Fig. 1. Further to this we undertook gel filtration of cell lysates to determine the apparent molecular mass of the mGFP-WDR34-containing complexes. Fig. 3D shows that using a calibrated Superose 6 column, we found that all detectable mGFP-WDR34 fluorescence eluted with the void volume of the column (Fig. 3D, fraction 15, 7.9 ml) corresponding to high molecular weight components (~1 x 10^7 Da). GFP by contrast eluted within the range of 4-7 x 10^4 Da (Fig. 3D, fractions 33-37). As with the sucrose gradients, it is evident that there is a significant fraction of mGFP-WDR34 (and also mGFP as a degradation product from this) that elutes in low molecular weight and low density fractions. This complicates analysis of the exact proportion of mGFP-WDR34 that is contained within the dynein-2 complex.

We have shown previously that defects in cilia formation and function are evident following depletion of Tctex-1 (Palmer et al., 2011) and WDR34 (Asante et al., 2013) in vitro. Specifically, siRNA-mediated depletion of either of these genes results in a reduced number of cells that produce cilia but also a lengthening of those cilia that remain. To determine whether this was true of the newly identified dynein-2 subunits, we first examined the role of WDR60. The biochemical data shown above suggest that WDR34 and WDR60 might act within the same dynein-2 complex. We found that endogenous WDR60, like WDR34, also localized around the centrosome (Fig. 4A) and that this localization was lost following depletion of either WDR60 itself or of WDR34 (Fig. 4A) suggesting that they function together. Consistent with this, depletion of either WDR34 or WDR60 resulted in a loss of WDR34 labelling around the centrosome (Fig. 4B). Depletion of WDR60 clearly led to one of two phenotypes, an increase in cilia length (example shown in Fig. 4C for WDR60 siRNA #1) or a complete loss of an extended axoneme (example shown in Fig. 4C for WDR60 siRNA #2), both of which were associated with a loss of labelling of WDR60 (Fig. 4C). Quantitation of these data showed that loss of WDR60 resulted in a significant reduction in the proportion of ciliated cells (Fig. 4D), with a clear increase in length of the remaining cilia (Figure 4E); this is highly similar to what we observed following depletion of WDR34 (Asante et al, 2013). The increase in cilia length is particularly evident on a cumulative frequency plot (Fig. 4F). Immunoblotting confirmed the efficacy of WDR34 and WDR60 siRNAs (Fig. 4G) as well as revealing that WDR34 and WDR60 were reciprocally required for stability of the other. We then repeated our analysis using both WDR34 and WDR60 siRNAs. Of note, double depletion of both WDR34 and WDR60 did not further exacerbate the cilia phenotypes seen (Fig. 4H, I, and J).

In our previous work, we showed that the localization of WDR34 to the pericentrosomal region was dependent on the function of the transmembrane Golgi matrix protein giantin (Asante et al., 2013). If WDR34 and WDR60 are indeed in complex together then one would predict the same would hold true for WDR60. Fig. 5A shows that loss of giantin following siRNA depletion does indeed result in a reduction of WDR60 labelling at the centrosome (quantified in Fig. 5B). The degree of loss of giantin also correlated with the intensity of labelling of WDR60 in the pericentrosomal area (Fig. 5C, quantified in 5D) as we have seen previously for WDR34. The siRNA duplexes used to target giantin have been characterized previously (Asante et al., 2013) with siRNA #1 being more effective than siRNA #2. This also is evident from the data seen in Fig. 5D.

We then used similar assays to test the role of NudCD3 in ciliogenesis. We suppressed expression of NudCD3 using siRNA (Fig. 6A) and found that this diminishes the ability of cells to generate primary cilia (Fig. 6B, quantified in 6C). Furthermore, those cilia that were seen to remain were found to be longer (Fig. 6D, quantified in 6E with cumulative frequency plots shown in 6F). Consistent with our other data, depletion of NudCD3 also resulted in a loss of WDR34 around the pericentrosomal region (Fig. 6G, quantified in 6H) without affecting the localization of OFD1 (Fig. 6I) or pericentrin (Fig. 6B).

We then examined the role of TCTEX1D2 using siRNA transfection. Figure 7A shows the efficacy of three individual siRNAs measured by quantitative PCR. As shown in Fig. 7B and quantified in Fig. 7C, depletion of TCTEX1D2 results in longer cilia following serum withdrawal. In all cases we can detect a statistically significant increase in cilia length following TCTEX1D2 depletion. This is more evident in cumulative frequency plots (Fig. 7D). Notably, the ability of cells to form primary cilia is not obviously affected following TCTEX1D2 depletion (Fig. 7E).

165

DISCUSSION

Here, we provide the first molecular characterization of the human dynein-2 complex. Our data build on previous reports to provide a comprehensive picture of the subunit composition of this motor as summarized in the schematic in Figure 8. Our data show that human dynein-2 contains both WDR34 and WDR60 intermediate chain subunits. Individual cytoplasmic dynein-1 complexes contain two copies of the same intermediate chain and same light intermediate chain (typically DYNC1I2 in most cells, DYNC1I1 in neurons). Biochemical experiments using *Chlamydomonas* showed that FAP133 (WDR34) co-purifies and co-immunoprecipitates with other dynein-2-specific (heavy chain and light intermediate chain) subunits and with the dynein light chain, LC8. These data are consistent with FAP133 being a dynein-2 intermediate chain subunit (Rompolas et al., 2007) and led the authors to propose a model in which dynein-2 contains two copies of FAP133, analogous to the dynein-1 complex containing two copies of the intermediate chain. Our data suggest that in fact dynein-2 contains both WDR34 and WDR60 intermediate chains. This asymmetry has the potential to provide more functional specialization and greater control of motor function. Furthermore, WDR60 is a larger protein than either WDR34 or the IC subunits of dynein-1. It is tempting to speculate that this asymmetry is related to its function. Evidence, primarily from *Chlamydomonas*, demonstrates that axonemal dyneins contain multiple intermediate chains within the same complex (Mitchell and Rosenbaum, 1986; King et al., 1991). For example, Inner arm dynein I1 contains three intermediate chain subunits IC140, IC138, and IC97. Dimeric outer arm dynein from *Chlamydomomas* contains two intermediate chain subunits IC1 and IC2. As such cytoplasmic dynein-2 shows similarities to axonemal dyneins. This could relate to the association of these motors with axonemal microtubules.

It is interesting to note that while mGFP-WDR34 is detectable in cilia, labelling with currently available antibodies does not detect this pool (also see (Asante et al., 2013; Schmidts et al., 2013a)). These data suggest that the antibody epitope is occluded within cilia. This could be due to dynein binding to the axonemal microtubules or to other factors such as the IFT-A particle. The pericentrosomal labelling could indicate a different set of associated factors at the cilia base or that dynein-2 is assembled at the base of primary cilia exposing a pool of WDR34. We also cannot rule out that WDR34 itself has some function outside of the context of the assembled dynein-2 complex; our gel filtration data are consistent with the presence of mGFP-WDR34 within or in association with high molecular weight complexes. Our co-immunoprecipitation data argue in favour of all WDR60 being in association with WDR34. Sucrose density gradient centrifugation shows that there is a proportion of WDR34 outside of the dynein-2 complex that could act in isolation, or in a heterodimeric complex with WDR60, or in some other complex. Our gel filtration experiments are also consistent with this. While we have not been able to monitor the dynein-2 heavy chain by immunoblotting, our previous work with dynein-1 showed that loss of the intermediate chain subunit did not result in concomitant loss of the heavy chain (Palmer et al., 2011). These data also therefore do not rule out the possibility of a functional dynein-2 heavy chain without associated WDR34 and WDR60. However, the importance of these intermediate chain subunits for dynein-2 function is underscored by their conservation through evolution (Wickstead and Gull, 2007). Mutation of either WDR34 (Huber et al., 2013; Schmidts et al., 2013a) or WDR60 (Rompolas et al., 2007) causes skeletal ciliopathies with a similar phenotype to that seen following mutation of the dynein-2 heavy chain (Dagoneau et al., 2009; Schmidts et al., 2013b). These findings that WDR34 cannot compensate for loss of function of WDR60 and vice versa are consistent with our model that both act together in the same dynein-2 complex. We conclude that the full dynein-2 complex including both WDR34 and WDR60 operates in IFT within cilia.

Analysis of dynein light chain function in the context of cilia biology provides important clues to the way in which dynein-2 assembles and controls protein distribution within, and retrograde exit from, cilia. The association of Tctex-1 with dynein-2 complexes was predicted from our previous work (Palmer et al., 2011). Here, we now also identify the TCTEX1D2 light chain (Tctex-2) as a light chain for dynein-2, not present in dynein-1. Tctex-2 has previously been found to control outer arm dynein assembly in *Chlamydomonas* flagella (Patel-King et al., 1997; Pazour et al., 1999). Evidence suggests that, unlike other dynein light chains, TCTEX1D2 is monomeric (DiBella et al., 2001). One possibility is that a single copy of TCTEX1D2 binds WDR34 with an alternative light chain (or a functionally similar protein) binding to WDR60. This could diversify the regulation of dynein-2 function and potentially influence the cargo binding capabilities of the complex. Our data show that a reduction of TCTEX1D2 expression results in an increase in cilia length similar to that which we observed following depletion of WDR34, WDR60, and giantin. Of note, TCTEX1D2 depleted cells still form cilia. We cannot reject the idea that TCTEX1D2 is required for cilia formation as these experiments are only depletion

experiments and not a complete knockout. The moderate phenotype seen here in vitro might also reflect some functional overlap with other dynein light chains in this system. It remains unclear whether dynein light chains act in directing dynein complex assembly and/or in cargo binding. It is also important to note that our in vitro assays reporting an elongation of cilia do not reflect the situation in vivo where the primary failure appears to be in ciliogenesis i.e. the formation of the axoneme. Our interpretation is that our siRNA experiments reflect a defect in retrograde IFT.

NudCD3 has been shown to influence the assembly and stability of the dynein-1 complex (Zhou et al., 2006) and localizes to centrosomes (Cai et al, 2009). Our data are consistent with it playing a similar role with dynein-2. We have not been able to detect NudCD3 in cilia by immunofluorescence or using epitope tagged forms (Zhou et al., 2006) arguing in favour of a role in assembly of dynein-2 within the main body of the cell. Association of NudCD3 with both cytoplasmic dynein complexes makes analysis of its function more complex. Its role in ciliogenesis is most likely linked to its interaction with dynein-2. However, we would not expect to find mutations in this gene associated with ciliopathies as a loss-of-function would compromise dynein-1, likely leading to cell death. We also identified the related NudC protein in our proteomics (Supplementary Table 1C) but as yet we have not investigated further the role of NudC in cilia or dynein-2 function but we note that NudC has been shown to localize to motile cilia (Pedersen et al., 2007).

In our experiments we typically observe two outcomes following siRNA-mediated suppression of dynein-2 subunits: fewer cilia but those that remain being longer. We interpret this as a threshold effect of our in vitro experiments. Partial loss of function compromises retrograde IFT and results in longer cilia (as anterograde IFT continues to deliver axonemal and other components to the tip). More effective depletion results in an inability of cells to form cilia with limited or no extension of the axoneme. It is also important to note that longer cilia have not typically been described for patient mutations, indeed cells from patients with WDR34 mutations show shorter cilia on average (Huber et al., 2013). However, phenotypic variability, with some cells failing to extend an axoneme while others can, has been seen in fibroblasts from patients with WDR60 mutations (McInerney-Leo et al., 2013). This distinction between in vitro and in vivo outcomes necessitates caution in interpretation of data. Nonetheless, our data show clear roles for WDR34, WDR60, and TCTEX1D2 within the context of the dynein-2 complex.

It is also significant to note that we do not detect any association of dynein-2 with many known regulators of cytoplasmic dynein-1 and axonemal dynein, including dynactin and LIS1. It is however important to note that while our work does show that dynactin and LIS1 do not stably associate with dynein-2, our data do not preclude that they do not associate transiently with dynein-2. For example, LIS1 acts in the initiation of dynein-1 motility but does not remain associated with it during organelle transport (Egan et al., 2012). Consistent with such a model, although we do not detect LIS1 in association with dynein-2 by co-immunoprecipitation, we can localize LIS1 to primary cilia by immunofluorescence (unpublished observations). LIS1 is also believed to act in generating a persistent force state of dynein to aid its function in moving heavy loads (McInerney-Leo et al., 2013). While such functions are required of dynein-1 (for example in nuclear migration) and axonemal dyneins (in generating the force of cilia and flagellar beating) it is conceivable that such large cargo loads are not part of the cargo repertoire transported by dynein-2. LIS1, dynactin and BICD family proteins likely cooperate to direct association of dynein with cargo and subsequent motility (Egan et al., 2012; Splinter et al., 2012; Wang et al., 2013; Moon et al., 2014). The absence of dynactin suggests that other as yet unidentified accessory factors likely act in cooperation with dynein-2 in linking the motor to its cargo. Other recent in vitro reconstitution experiments have shown that dynein-1 requires the association of both dynactin and another accessory factor such as BICD2 to induce a processive state (McKenney et al., 2014; Schlager et al., 2014). Dynein-2 is also likely to be a processive motor and it is tempting to speculate that additional factors are required to induce processivity, possibly the IFT-A complex itself. Further biochemical and biophysical analysis would undoubtedly help to address such questions.

In conclusion, our characterization of the subunit composition of cytoplasmic dynein-2 defines a requirement for both WDR34 and WDR60 in dynein-2 function, explaining why mutations in either gene cause disease. Furthermore, this work identifies TCTEX1D2 as a candidate ciliopathy gene.

Materials and Methods

All reagents were purchased from Sigma-Aldrich (Poole, UK) unless otherwise stated.

Growth of culture cells

Human telomerase immortalized retinal pigment epithelial cells (hTERT-RPE1) were maintained in DMEM-F12 supplemented with 10% FCS (Life Technologies, Paisley, UK) containing supplemented 1% L-glutamine and 1% essential amino-acids. Cells were seeded onto 35 mm glass bottom dishes (MatTek, Ashland, MA).

Ciliogenesis assay

On reaching confluence, hTERT-RPE1 cells were rid of serum by washing twice with PBS and incubated at 37 °C/5% CO_2 for 24–48 h in serum-free medium to induce cell cycle exit and subsequent cilium assembly. Cells were fixed and typically labelled with anti-acetylated tubulin to mark primary cilia. Cilia lengths were measured using the Fiji implementation of Image J (Schindelin et al, 2012).

Source of antibodies

Antibodies used include: rabbit polyclonal anti-WDR60 (HPA020607), rabbit polyclonal anti-NudCD3 (HPA019136), rabbit polyclonal anti-ODF2 (HPA001874), mouse monoclonal anti-acetylated tubulin (T6793) and mouse monoclonal anti-γ-tubulin (T6557) (all from Sigma-Aldrich); rabbit polyclonal anti-giantin (PRB-114C), mouse monoclonal anti-GFP (MMS-118P) and rabbit polyclonal anti-pericentrin (PRB-432C) (all from Covance, CA); mouse monoclonal anti-p150glued (610473) and mouse monoclonal anti-p50dynamitin (BD 611003) (both from BD Biosciences, Oxford, UK); rabbit polyclonal anti-WDR34 (NBP1-88805, Novus Biologicals, Cambridge, UK), rabbit polyclonal anti-Tctex1 (sc-28537, Santa Cruz Biotechnology, Dallas, TX), mouse monoclonal anti-GAPDH (ab9484, Abcam, Cambridge, UK), rabbit polyclonal anti-TCTEX1D2 (ab139804, Abcam), mouse monoclonal anti-DIC74 (MAB1618, Millipore, Feltham, UK), rabbit polyclonal anti-Lamin A/C (2032, Cell Signaling Technologies, Hitchin UK), rabbit polyclonal anti-OFD1 (a generous gift from Andrew Fry, University of Leicester, UK), and rabbit polyclonal anti-LIS1 (A300-409A, Bethyl Laboratories, from Cambridge Bioscience, Cambridge, UK). Cy2-conjugated donkey anti-mouse (715-225-151), Cy3-conjugated donkey anti-rabbit (711-165-152), peroxidase-conjugated donkey anti-mouse IgG (715-035-150) and peroxidase-conjugated donkey anti-rabbit IgG (711-035-150) were supplied by Jackson ImmunoResearch (from Stratech Scientific, Newmarket, UK). IRDye 800CW donkey anti-mouse (926-32212) and IRDye 680 donkey anti-rabbit (926-32223) were from Li-Cor (Cambridge, UK).

Cloning of mGFP-WDR34, generation of lentiviruses and stable cell lines

The human WDR34 gene (RefSeq: NM_052844.3) was amplified from the Origene cDNA (SC319901, Cambridge Bioscience) by PCR using Phusion™ high-fidelity DNA polymerase PCR kit (New England BioLabs, Hitchin, UK) with forward primer (5'-GGAA-CTCGAG-ATGGCAACCCGCGCGCAGCC-3') and reverse primer (3'-GAAA-GAATTC-TCAGGCCGCCACCTCTGCTGC-5'), containing the XhoI and EcoRI restriction sites, respectively. The PCR product was sub-cloned into a modified pLVX-Puro vector (Clontech, Mountain View, CA) that includes the mGFP sequence flanked by XhoI and EcoRI restriction sites. The resultant pLVX-Puro-mGFP-WDR34 CDNA was amplified in XL10-Gold ultracompetent bacterial cells (Stratagene) and harvested from the bacterial cells using QIAprep Spin Miniprep Kit (Qiagen, Manchester, UK). All plasmid minipreps were validated by restriction analysis and subsequently sequenced to facilitate secondary validation by sequence alignment analysis.

Lentiviral particles of pLVX-Puro-mGFP-WDR34 were produced in HEK293T cells using the Lenti-X™ HTX Packaging System (Clontech), and low passage hTERT-RPE1 cells transduced with the resultant viral supernatant, strictly according to manufacturer's directives. 48 h post-transduction, confluent cells were subcultured into 10 % FBS supplemented DMEM F-12 HAM (Sigma-Aldrich, Poole, UK) containing 5 μg/ml puromycin. Cells were maintained in 0.25 μg/ml puromycin after this.

Proteomics

3 x 15 cm dishes each of hTERT-RPE1-mGFP (control) and hTERT-RPE1-mGFP-WDR34 cells were serum-starved for 24 h at confluence to induce ciliogenesis. Cells were briefly washed twice with 20 mL ice-cold PBS per dish and PBS drained

off completely by leaning the dishes at ~60° for ~10 s. 500 µL of ice-cold lysis buffer 1 (10 mM Tris-HCl [pH=7.4], 50 mM NaCl, 0.5 mM EDTA, 1.0 % Igepal [CA-630, Sigma], containing freshly added 1mM phenylmethane sulfonylfluoride [PMSF] and 1x EDTA-free Protease Inhibitor Cocktail Set V [539137, Millipore, UK]) was added to the cells and the cells scraped off the dish floor into 2 mL tubes. Cells were lysed by incubation with the buffer on a rotor at 4 °C/30 min. Lysates were centrifuged at 20,000 g/4 °C/10 min and supernatants transferred into pre-cooled 2 mL eppendorf tubes.

Equilibration of GFP nano-trap beads and immunoprecipitation

20 µL of resuspended GFP nano-trap beads (Chromotek, Planegg-Martinsried, Germany) per sample was added to ice-cold 500 µL dilution buffer (10 mM Tris-HCl [pH=7.4], 50 mM NaCl, 0.5 mM EDTA, freshly added 1 mM PMSF and 1x EDTA-free Protease Inhibitor Cocktail), spun down at 2700 g/2 min/4 °C and the supernatant discarded. This wash was repeated 2 additional times. The cell lysate supernatants were added to the equilibrated beads and incubated on a rotor 4 °C/2 h.

Sample preparation for mass spectrometry

At the end of the incubation the tubes were centrifuged at 2000 g/2 min/4 °C and the supernatants discarded. 500 µL of ice-cold dilution buffer was added to the protein-bound beads (pellets), the tubes inverted gently ~10 times to resuspend contents and spun down at 2000 g/2 min/4 °C. This wash was repeated 2 more times after which the beads were resuspended in 50 µL 2X lithium dodecyl sulphate (LDS) sample buffer (NP0007, Life Technologies Ltd, Paisley, UK) (106 mM Tris-HCl, 141 mM Tris-base, 2 % LDS, 10 % Glycerol, 0.51 mM EDTA, 0.22 mM SERVA® Blue G250, 0.175 mM Phenol Red [pH 8.5]) containing 1x Nupage® sample reducing agent (500 mM dithiothreitol) (NP0004). The beads were boiled at 95 °C/10 min to denature proteins and dissociate precipitated proteins from the GFP nano-trap beads and the tubes immediately placed on ice for 1 min to condense vaporised contents. The tubes were centrifuged at 2700 g/2 min/4 °C, to sediment beads and the supernatants collected into fresh 1.5 mL eppendorf tubes. These samples were submitted to the University of Bristol's proteomics facility for mass spectrometry analysis.

Mass spectrometry

Samples were run on a 10 % acrylamide gel to separate proteins. Each gel lane was cut into 6 slices and each slice put through in-gel tryptic digestion in a ProGest automated digestion unit (Digilab UK). An Ultimate 3000 nano HPLC system operated in line with an LTQ-Orbitrap Velos mass spectrometer (Thermo Scientific) was employed in fractionating the resulting peptides. Summarily, peptides in 1% (vol/vol) formic acid were injected onto an Acclaim PepMap C18 nano-trap column (Thermo Scientific). The peptides were washed with 0.5 % (vol/vol) acetonitrile in 0.1 % (vol/vol) formic acid and resolved on a 250 mm × 75 µm Acclaim PepMap C18 reverse phase analytical column (Thermo Scientific) over a 150 min organic gradient composed of 7 gradient segments. Peptides were run over the column through the following sequential gradients: 1-6 % solvent B/1 min (solvent B = aqueous 80 % acetonitrile in 0.1 % formic acid; solvent A = 0.1 % formic acid), 6-15 % B/58 min, 15-32 % B/58 min, 32-40 % B/5 min, 40-90 % B/1 min, 90 % B/6 min and finally, 1 % B/1 min; with a flow rate of 300 nL/min. Peptides were subjected to 2.1 kV nano-eloctrospray ionisation from a 30 µm (internal diameter) stainless steel emitter (Thermo Scientific) with a capillary temperature of 250 °C. An LTQ-Orbitrap Velos mass spectrometer operated by the Xcalibur 2.1 software (Thermo Scientific) in data-dependent acquisition mode was used to acquire tandem mass spectra of the peptides. Survey scans were analysed at 60,000 resolution (at m/z 400) within the mass range m/z 300-2000, and the top 20 multiple-charged ions in each duty cycle selected for MS/MS in the LTQ linear ion trap. Charge state filtering, which excludes unassigned precursor ions from fragmentation, and dynamic exclusion (repeat count, 1; repeat duration, 30 s; exclusion list size, 500) were applied. The following fragmentation conditions were set in the LTQ: 40 % normalised energy of collision, 0.25 activation q, 10 ms activation time, and a minimum ion selection intensity of 500 counts.

Proteome Discoverer software (version 1.2, Thermo Scientific) was used to process and quantify the raw data files, which were then searched against the UniProt human database (122604 sequences) using the SEQUEST algorithm (version 28, revision 13). Tolerances of 10 ppm and 0.8 Da were set for peptide precursor mass and MS/MS, respectively. Cysteine carbamidomethylation (+57.0214) and methionine oxidation were included in the search criteria as fixed modifications and variable modifications, respectively. Searches were performed with full tryptic digestion allowing a maximum of 1 missed cleavage. All peptide data was filtered to satisfy a 5 % false discovery rate (FDR) by enabling the reverse database search option. The Proteome Discoverer software creates a reverse "decoy" database

from the same protein database; peptides evading the initial filtering parameters that were derived from this decoy database are badged as false positive identifications. The minimum cross-correlation factor (Xcorr) filter was separately readjusted for each individual charge state to meet the predetermined target 5 % FDR, considering the number of random false positive matches from the reverse decoy database. Those proteins identified in Supplementary Table 1 were selected on the basis of being known components or well-characterized interactors of cytosplasmic dynein-1.

GFP-Trap immunoprecipitation

Cells were grown to confluence in 15 cm dishes and serum starved for 24 h. Cells were washed twice with ice-cold PBS, lysed with 500 µl ice-cold buffer (10 mM Tris-HCl pH=7.4, 50 mM NaCl, 0.5 mM EDTA, 1.0% Igepal CA-630, 1 mM PMSF and 1x Protease inhibitor cocktail) on rotator for 30 mins/4 ^{o}C and lysate supernatant collected after centrifuging at 20,000 g/10 mins/4 ^{o}C. Lysate supernatants were incubated with equilibrated GFP nano-trap beads (Chromotek) on rotator for 90 mins/4 ^{o}C after which the beads were washed three times with 500 µl dilution buffer (10 mM Tris-HCl pH=7.4, 50 mM NaCl, 0.5 mM EDTA, 1 mM PMSF and 1x Protease inhibitor cocktail) by centrifuging at 2000 g/2 mins/4 ^{o}C. Beads were resuspended in 50 µl 2x LDS sample buffer (Life Technologies) containing sample reducing agent (Life Technologies) and boiled at 95 ^{o}C/10 mins, followed by SDS-PAGE and immunoblotting as described below.

Small interfering RNA transfection

Cells were siRNA-transfected by calcium phosphate method at 3% CO_2 (Chen & Okayama, 1988). The medium was changed 20 hours post-transfection and cells were washed with PBS and were incubated for 72 hours (at 37°C and 5% CO_2) with fresh supplemented media. SiRNA duplexes were designed using online algorithms of, and subsequently synthesized by, MWG-Eurofins. BLAST search was performed for these duplexes against the non-redundant database to determine their specificity. Lamin A/C or luciferase GL2 were depleted as targeted controls.

Sequences used were as follows:

Giantin was depleted with giantin siRNA (#1) ACUUCAUGCGAAGGCCAAATT and giantin siRNA (#2) AGAGAGGCUUAUGAAUCAATT. Duplexes for suppressing WDR34 were (#1) GAUGGUGUCUUGUCUGUAU and (#2) GCUGUUUGAUCUCCAGAAA. WDR60 was targeted with (#1) CCAUUUGGAGAACCAAUAU and (#2) CAUGGUAUAAGACCAGUGA. Duplexes targeting NUDCD3 include (#1) GUGAUGCAGUGGUGUGAGA and (#2) GAGAAGGCAGGAACUUGAA. Luciferase GL2 (CGUACGCGGAAUACUUCGAUU) and lamin A/C (CUGGACUUCCAGAAGAACA) were used as targeted negative and positive controls, respectively. All siRNAs were purchased from MWG Eurofins (Ebersberg, Germany). TCTEX1D2 was depleted with (#1) AGAGGUGAAGGAGUAUUCATT, (#2) UGCUGAAUAUUCUCCAGAATT and (#3, targeting 3'UTR) AGGACAUGACCAUGAAGAATT

Quantitative PCR

RNA was extracted from transfected cells using a Qiagen RNeasy purification kit according to the manufacturer's instructions (Qiagen, Manchester, UK) . cDNA was generated using an SuperScript^{TM} III First Strand Synthesis System (Life Technologies). DNA was amplified under the following conditions: 95^{o}C for 10 minutes then 30 cycles of 95^{o}C for 30 seconds, 55^{o}C for 30 seconds, 70^{o}C for 15 seconds. Amplification was monitored by incorporation of SYBR® Green (Finnzyme, Espoo, Finland) and analysed on a BioRad Opticon 2 PCR system (BioRad, Hemel Hempstead, UK). Gene expression was quantified by the $\Delta\Delta$CT method (Livak & Schmittgen, 2001) normalizing against GAPDH. Single product amplification was verified by performing melting curve analysis and gel electrophoresis. Primers (MWG Eurofins) used were as follows: TCTEX1D2 forward primer: 5'- GGAGCCCGAGAACACCTATATT-3'; reverse primer: 5'-GCTGAGGCATTTCTTCTGGAGA-'; GAPDH forward primer: 5'-ATCCCATCACCATCTTCCAG-3'; reverse primer: 5'-CCATCACGCCACAGTTTCC-3'.

Sucrose density gradient centrifugation

Cells were grown and lysed as described for the GFP-trap experiment and lysate supernatants layered onto 5-40% or 5-20% continuous sucrose gradient columns. The former were poured using a Perspex gradient mixer, the latter using Biocomp isopycnic gradient forming tube caps (10 mm isopycnic long caps, Biocomp from Wolf Laboratories,

Manchester, UK). Gradients were centrifuged at 23,700 rpm (96119 x*g*)/18 h/4 °C in a TH-641 swinging bucket rotor (Thermo Scientific). Proteins were precipitated with 250 µl or 125µl 100% trichloroacetic acid at 4 °C /1 h from 1 ml or 500 µl column fractions respectively, pelleted by centrifuging at 13,200 rpm/5 mins/4 °C, and washed three times with 150 µl ice-cold acetone. The acetone was chased off by incubation at room temperature for 30 minutes and pellets resuspended in 1x LDS sample buffer containing reducing agent.

Immunoblotting

For immunoblots to validate siRNA efficacy, cells were lysed and samples were separated by SDS-PAGE followed by transfer to nitrocellulose membranes; primary antibodies were detected using HRP-conjugated secondary antibodies (Jackson ImmunoResearch, West Grove, PA) and enhanced chemiluminescence (ECL, GE Healthcare, Cardiff, United Kingdom). Immunoblots in Fig. 6 were developed using an Odyssey Sa imager (Li-Cor, Cambridge, UK).

GEL FILTRATION

The following buffer was used for gel filtration: 30 mM HEPES (pH 7.0), 150 mM KOAc, 2 mM $MgSO_4$, 0.68 M glycerol, 2 mM DTT. A 24 ml Superose 6 column (GE Healthcare) was calibrated using 70S ribosome, apoferritin, b-amylase, bovine serum albumin and carbonic anhydrase. Cells expressing either GFP or mGFP-WDR34 were lysed at 4°C using a ball bearing cell homogenizer with 10 µm clearance (Isobiotec, Heidelberg) in gel filtration buffer and cleared by centrifugation for 30 minutes at 25,000 x*g*. Fractions (0.5ml each) were collected and fluorescence of each sample measured using a Cary Eclipse Fluorescence Spectrophotometer (Agilent Technologies, Santa Clara, CA) at 25°C with excitation at 490 nm (5 nm excitation slit) and emission scanning 500-600 nm with 5 nm emission slits.

Immunolabelling and microscopy

Medium was removed and cells were subsequently washed with PBS. Cells were then fixed using cold methanol for 4 minutes at -20°C. For images in Figure 1E and 1F, cells were fixed with 4% paraformaldehyde in PBS, permeabilized with 0.1% Triton X-100 for 5 minutes and then washed in PBS. After two washes in PBS, cells were blocked using a 3% bovine serum albumin (BSA) in PBS for 30 minutes at room temperature. Three washes with PBS of 5 minutes each at room temperature were done after each of the primary and secondary antibody incubations. Nuclear staining was done using DAPI (4,6-Diamidino-2-phenylindole (Life Technologies) diluted at 1:5000 in distilled water) for 3 minutes at room temperature, cells were then rinsed twice in PBS. Cells were imaged using an Olympus IX-71 or IX-81 widefield microscope with a 63x 1.42 N.A. objective, and excitation and emission filter sets (Semrock, Rochester, NY) controlled by Volocity software (v. 4.3, Perkin-Elmer, Seer Green, UK).

Processing and quantification of image data and statistical analysis

Representative images are shown, all experiments were repeated independently at least three times each. Samples were compared using Kuskall-Wallis one-way analysis of variance with Dunn's post-hoc test using GraphPad Prism v 4. All images were prepared with Adobe Photoshop and Adobe Illustrator. All data and resulting statistical analyses arise from 3 independent experiments.

Acknowledgements

We would like to thank the Wolfson Foundation, MRC, and University of Bristol for establishing and maintaining the University of Bristol Wolfson Bioimaging Facility and Mark Jepson, Alan Leard, and Katy Jepson for their help with training. We are especially grateful to Mark Szczelkun and Paul Curnow for their help with gel filtration experiments and to Ariel Blocker for tips on sucrose density gradient formation. This work was funded by the UK Medical Research Council (a PhD studentship [G1000383-1/1] and research grant [MR/K018019/1] to D.J.S.) and the University of Bristol. The authors declare no competing interests.

Contributions

D.A. performed experiments and analyzed data; N.S. performed experiments and analyzed data; D.J.S. conceived and directed the project, analyzed data, and wrote the manuscript. All authors reviewed and contributed to the writing of the manuscript.

FIGURE LEGENDS

Figure 1: Localization of mGFP-WDR34. (A) mGFP-WDR34 (green) localizes to a cytosolic pool and to primary cilia colocalizing with acetylated tubulin (red). (B) γ-tubulin labelling, (C) ODF2, and (D) OFD1 (red in each case) demonstrate the accumulation of mGFP-WDR34 at the base of the cilium with some labelling evident along its length. (E) Cells expressing mGFP-WDR34 were fixed with paraformaldehyde and labelled to detect acetylated tubulin and WDR34 as indicated. Two examples are shown. (F) Cells expressing GFP were processed as in (E) to demonstrate an absence of GFP from primary cilia. Bars (all panels) = 5 µm.

Figure 2: Immunoprecipitation from serum-starved RPE1 cells stably expressing either mGFP or mGFP-WDR34. GFP-traps of cells expressing mGFP alone or mGFP-WDR34 were separated by SDS-PAGE and immunoblotted to detect (A) WDR34, (B) WDR60, (C) IC74 (DYNC1I2), (D) GAPDH, (E) $p150^{Glued}$, (F) $p50^{dynamitin}$, (G) LIS1, (H) Tctex-1, (I) NudCD3, or (J) TCTEX1D2 as indicated. Molecular weight markers are shown (kDa). In each case the lanes show I = input, U = unbound fraction, B = bound fraction as indicated.

Figure 3: Sucrose density gradient centrifugation of cell lysates from RPE1 cells. (A) RPE1 cells were lysed and loaded onto a 5-40% sucrose density gradient. After centrifugation, 1 ml fractions were removed from the gradient and probed by immunoblotting to determine the distribution across the gradient of DIC74 (DYNC1I2), WDR34, or GAPDH. (B) RPE1 cells stably expressing (B) GFP or (C) mGFP-WDR34 were lysed and loaded onto a 5-20% sucrose density gradient. Twenty 500 µl fractions were collected post-centrifugation and alternate fractions analysed by SDS PAGE and immunoblotting for GFP, DIC74, GAPDH and WDR60. (D) Gel filtration of lysates from GFP expressing cells (gray bars) and mGFP-WDR34 expressing cells (black bars). Molecular mass calibration is shown below the graph aligned to the fraction numbers.

Figure 4: The stabilities of WDR34 and WDR60 are interdependent. (A, B) Cells were transfected with siRNA duplexes targeting WDR34 or WDR60 as indicated and following serum starvation, fixed and immunolabelled to detect acetylated tubulin and (A) WDR60 or (B) WDR34. (C) Cells depleted of WDR60 were effectively depleted (shown by loss of immunoreactivity around the centrosome) and labelling showed either longer cilia (example shown for WDR60-1) or a failure to generate cilia (example shown for WDR60-2). (D) Quantitation of the proportion of cells that produced cilia in response to 24 hours serum starvation. Asterisks indicate statistical significance (* $p<0.05$; ** $p<0.01$). (E) Lengths of remaining cilia were measured for control (GL2) or WDR60-depleted cell cultures. Bars show mean and s.d.; asterisks indicate statistical significance (*** $p<0.001$). (F) Distribution of cilium length represented as a cumulative frequency chart of the percentage of total cilia found in 0.25 µm bins. Data plotted is the same as in (E). (G) Immunoblotting confirmed the efficacy of WDR34 and WDR60 siRNAs. Immunoblotting for WDR34 following suppression of WDR60 and vice versa was also used to test interdependency of these subunits. Lamin A/C is included as a negative control, GAPDH as a loading control. Molecular weight markers are indicated (kDa). (H, I) Results were analysed to determine whether depletion of both WDR34 and WDR60 simultaneously could enhance the phenotypes seen in terms of (H) the number of cells producing cilia or (I) the length of remaining cilia. In both cases no additive effect is seen. Bars show mean and s.d.; asterisks indicate statistical significance (*** $p<0.001$). (J) Distribution of cilium length represented as a cumulative frequency chart of the percentage of total cilia found in 0.25 µm bins. Data plotted is the same as in (I). Bar (all panels) = 10 µm.

Figure 5: Suppression of giantin results in a loss of pericentrosomal WDR60. (A) Cells depleted of giantin were labelled to detect acetylated tubulin and WDR60. (B) The area of pericentrosomal WDR60 labelling was measured and plotted (arbitrary units; bars indicate mean and s.d.; asterisks indicate statistical significance: *** $p<0.001$). (C) The loss of pericentrosomal WDR60 labelling correlates with the efficacy of giantin suppression. (D) Data were quantified and the correlation tested using both Pearson's and Spearman coefficients. Colour coding indicates siRNA transfection as indicated. Bar (all panels) = 10 µm.

Figure 6: NudCD3 is required for ciliogenesis and cilia length control. Two independent siRNA duplexes targeting NudCD3 were used. (A) Immunoblots show tubulin as a loading control, lamin A/C as a siRNA control and NudCD3. (B) Cells were immunolabelled to detect pericentrin and acetylated tubulin. Enlargements highlight the failure to extend cilia from the basal body in NudCD3-depleted cells. (C) The proportion of ciliated cells was quantified; asterisks indicate

statistical significance (* p<0.05). (D) Further examples of NudCD3 depleted cells show those in which cilia are evident. (E) Quantitation shows that in cells depleted of NudCD3 that extended cilia, these were longer than those seen in control cells. Bars show mean and s.d.; asterisks indicate statistical significance (*** p<0.001). (F) Distribution of cilium length represented as a cumulative frequency chart of the percentage of total cilia found in 0.25 µm bins. Data plotted is the same as in (E). (G) Depletion of NudCD3 results in a loss of pericentrosomal WDR34 (red) as shown by immunofluorescence. The centrosome and cilia are labelled with acetylated tubulin. (H) Data were quantified and statistical significance is indicated, ** = p<0.05, *** = p<0.01. (I) Suppression of NudCD3 does not affect the accumulation of OFD1 (red) around the centrosome (acetylated tubulin, green). Bar (all panels) = 10 µm.

Figure 7: TCTEX1D2 depletion increases cilia length. RPE1 cells were depleted of TCTEX1D2 using 3 different siRNA duplexes as indicated and then serum starved for 24 hours prior to (A) analysis by QPCR or (B-D) fixation and immunolabelling to detect acetylated tubulin and pericentrin. (A) Relative TCTEX1D2 mRNA expression in transfected cells, as determined by RT-PCR. Error bars show s.e.m. (n=3). (B) Representative maximum intensity z-stack projections of control and depleted cells. Enlargements highlight the increase in cilia length upon TCTEX1D2 depletion. Bar = 10 µm. (C) Dot plot comparing cilia lengths in control and TCTEX1D2 depleted cells. Bars show mean and s.d. (p<0.001, n=3). (D) Distribution of cilium length represented as a cumulative frequency chart of the percentage of total cilia found in 0.25 µm bins. Data plotted is the same as in (B). (D) The percentage of ciliated cells found in control and TCTEX1D2 depleted cells. There is no consistent change following siRNA treatment. Error bars show s.e.m.

Figure 8: Schematic of cytoplasmic dynein-1 and dynein-2 complexes. Light intermediate chains are shown as hexagons, intermediate chains as extended ovals, and light chains as circles. Additional interacting partners are seen for dynein-1 (left) that are not associated with dynein-2 (right). NudCD3 associates with both cytoplasmic dynein complexes. It remains unclear whether TCTEX1D2 is present as a monomer or dimer within the complex.

References

Asante, D., Maccarthy-Morrogh, L., Townley, A. K., Weiss, M. A., Katayama, K., Palmer, K. J., Suzuki, H., Westlake, C. J. and Stephens, D. J. (2013). A role for the Golgi matrix protein giantin in ciliogenesis through control of the localization of dynein-2. *J. Cell Sci.* **126**, 5189-5197.

Criswell, P. S., Ostrowski, L. E. and Asai, D. J. (1996). A novel cytoplasmic dynein heavy chain: expression of DHC1b in mammalian ciliated epithelial cells. *J. Cell Sci.* **109 (Pt 7)**, 1891-1898.

Dagoneau, N., Goulet, M., Genevieve, D., Sznajer, Y., Martinovic, J., Smithson, S., Huber, C., Baujat, G., Flori, E., Tecco, L. et al. (2009). DYNC2H1 mutations cause asphyxiating thoracic dystrophy and short rib-polydactyly syndrome, type III. *Am. J. Hum. Genet.* **84**, 706-711.

DiBella, L. M., Benashski, S. E., Tedford, H. W., Harrison, A., Patel-King, R. S. and King, S. M. (2001). The Tctex1/Tctex2 class of dynein light chains. Dimerization, differential expression, and interaction with the LC8 protein family. *J Biol Chem* **276**, 14366-14373.

Egan, M. J., Tan, K. and Reck-Peterson, S. L. (2012). Lis1 is an initiation factor for dynein-driven organelle transport. *The Journal of cell biology* **197**, 971-982.

Faulkner, N. E., Dujardin, D. L., Tai, C. Y., Vaughan, K. T., O'Connell, C. B., Wang, Y. and Vallee, R. B. (2000). A role for the lissencephaly gene LIS1 in mitosis and cytoplasmic dynein function. *Nat. Cell Biol.* **2**, 784-791.

Gibbons, B. H., Asai, D. J., Tang, W. J., Hays, T. S. and Gibbons, I. R. (1994). Phylogeny and expression of axonemal and cytoplasmic dynein genes in sea urchins. *Mol. Biol. Cell* **5**, 57-70.

Grissom, P. M., Vaisberg, E. A. and McIntosh, J. R. (2002). Identification of a novel light intermediate chain (D2LIC) for mammalian cytoplasmic dynein 2. *Mol. Biol. Cell* **13**, 817-829.

Huangfu, D. and Anderson, K. V. (2005). Cilia and Hedgehog responsiveness in the mouse. *Proc. Natl. Acad. Sci. USA* **102**, 11325-11330.

Huber, C., Wu, S., Kim, A. S., Sigaudy, S., Sarukhanov, A., Serre, V., Baujat, G., Le Quan Sang, K. H., Rimoin, D. L., Cohn, D. H. et al. (2013). WDR34 Mutations that Cause Short-Rib Polydactyly Syndrome Type III/Severe Asphyxiating Thoracic Dysplasia Reveal a Role for the NF-kappaB Pathway in Cilia. *Am. J. Hum. Genet.*

Kardon, J. R. and Vale, R. D. (2009). Regulators of the cytoplasmic dynein motor. *Nature reviews. Molecular cell biology* **10**, 854-865.

King, S. M., Wilkerson, C. G. and Witman, G. B. (1991). The Mr 78,000 intermediate chain of Chlamydomonas outer arm dynein interacts with alpha-tubulin in situ. *J Biol Chem* **266**, 8401-8407.

Liem, K. F., Jr., Ashe, A., He, M., Satir, P., Moran, J., Beier, D., Wicking, C. and Anderson, K. V. (2012). The IFT-A complex regulates Shh signaling through cilia structure and membrane protein trafficking. *The Journal of cell biology* **197**, 789-800.

Liu, A., Wang, B. and Niswander, L. A. (2005). Mouse intraflagellar transport proteins regulate both the activator and repressor functions of Gli transcription factors. *Development* **132**, 3103-3111.

May, S. R., Ashique, A. M., Karlen, M., Wang, B., Shen, Y., Zarbalis, K., Reiter, J., Ericson, J. and Peterson, A. S. (2005). Loss of the retrograde motor for IFT disrupts localization of Smo to cilia and prevents the expression of both activator and repressor functions of Gli. *Dev. Biol.* **287**, 378-389.

McInerney-Leo, A. M., Schmidts, M., Cortes, C. R., Leo, P. J., Gener, B., Courtney, A. D., Gardiner, B., Harris, J. A., Lu, Y., Marshall, M. et al. (2013). Short-rib polydactyly and Jeune syndromes are caused by mutations in WDR60. *Am. J. Hum. Genet.* **93**, 515-523.

McKenney, R. J., Huynh, W., Tanenbaum, M. E., Bhabha, G. and Vale, R. D. (2014). Activation of cytoplasmic dynein motility by dynactin-cargo adapter complexes. *Science*.

Mitchell, D. R. and Rosenbaum, J. L. (1986). Protein-protein interactions in the 18S ATPase of Chlamydomonas outer dynein arms. *Cell Motil. Cytoskeleton* **6**, 510-520.

Moon, H. M., Youn, Y. H., Pemble, H., Yingling, J., Wittmann, T. and Wynshaw-Boris, A. (2014). LIS1 controls mitosis and mitotic spindle organization via the LIS1-NDEL1-dynein complex. *Hum. Mol. Genet.* **23**, 449-466.

Mukhopadhyay, S., Wen, X., Chih, B., Nelson, C. D., Lane, W. S., Scales, S. J. and Jackson, P. K. (2010). TULP3 bridges the IFT-A complex and membrane phosphoinositides to promote trafficking of G protein-coupled receptors into primary cilia. *Gene Dev* **24**, 2180-2193.

Palmer, K. J., MacCarthy-Morrogh, L., Smyllie, N. and Stephens, D. J. (2011). A role for Tctex-1 (DYNLT1) in controlling primary cilium length. *Eur. J. Cell Biol.* **90**, 865-871.

Paschal, B. M. and Vallee, R. B. (1987). Retrograde transport by the microtubule-associated protein MAP 1C. *Nature* **330**, 181-183.

Patel-King, R. S., Benashski, S. E., Harrison, A. and King, S. M. (1997). A Chlamydomonas homologue of the putative murine t complex distorter Tctex-2 is an outer arm dynein light chain. *The Journal of cell biology* **137**, 1081-1090.

Patel-King, R. S., Gilberti, R. M., Hom, E. F. and King, S. M. (2013). WD60/FAP163 is a dynein intermediate chain required for retrograde intraflagellar transport in cilia. *Mol. Biol. Cell* **24**, 2668-2677.

Pazour, G. J., Koutoulis, A., Benashski, S. E., Dickert, B. L., Sheng, H., Patel-King, R. S., King, S. M. and Witman, G. B. (1999). LC2, the chlamydomonas homologue of the t complex-encoded protein Tctex2, is essential for outer dynein arm assembly. *Mol. Biol. Cell* **10**, 3507-3520.
Pedersen, L. B., Rompolas, P., Christensen, S. T., Rosenbaum, J. L. and King, S. M. (2007). The lissencephaly protein Lis1 is present in motile mammalian cilia and requires outer arm dynein for targeting to Chlamydomonas flagella. *J. Cell Sci.* **120**, 858-867.
Pfister, K. K., Fisher, E. M., Gibbons, I. R., Hays, T. S., Holzbaur, E. L., McIntosh, J. R., Porter, M. E., Schroer, T. A., Vaughan, K. T., Witman, G. B. et al. (2005). Cytoplasmic dynein nomenclature. *The Journal of cell biology* **171**, 411-413.
Rompolas, P., Pedersen, L. B., Patel-King, R. S. and King, S. M. (2007). Chlamydomonas FAP133 is a dynein intermediate chain associated with the retrograde intraflagellar transport motor. *J. Cell Sci.* **120**, 3653-3665.
Rothbauer, U., Zolghadr, K., Tillib, S., Nowak, D., Schermelleh, L., Gahl, A., Backmann, N., Conrath, K., Muyldermans, S., Cardoso, M. C. et al. (2006). Targeting and tracing antigens in live cells with fluorescent nanobodies. *Nat Methods* **3**, 887-889.
Schlager, M. A., Hoang, H. T., Urnavicius, L., Bullock, S. L. and Carter, A. P. (2014). In vitro reconstitution of a highly processive recombinant human dynein complex. *Embo J.*
Schmidts, M., Vodopiutz, J., Christou-Savina, S., Cortes, C. R., McInerney-Leo, A. M., Emes, R. D., Arts, H. H., Tuysuz, B., D'Silva, J., Leo, P. J. et al. (2013a). Mutations in the gene encoding IFT dynein complex component WDR34 cause Jeune asphyxiating thoracic dystrophy. *Am. J. Hum. Genet.* **93**, 932-944.
Schmidts, M., Arts, H. H., Bongers, E. M., Yap, Z., Oud, M. M., Antony, D., Duijkers, L., Emes, R. D., Stalker, J., Yntema, J. B. et al. (2013b). Exome sequencing identifies DYNC2H1 mutations as a common cause of asphyxiating thoracic dystrophy (Jeune syndrome) without major polydactyly, renal or retinal involvement. *J. Med. Genet.* **50**, 309-323.
Splinter, D., Razafsky, D. S., Schlager, M. A., Serra-Marques, A., Grigoriev, I., Demmers, J., Keijzer, N., Jiang, K., Poser, I., Hyman, A. A. et al. (2012). BICD2, dynactin, and LIS1 cooperate in regulating dynein recruitment to cellular structures. *Mol. Biol. Cell* **23**, 4226-4241.
Wang, S., Ketcham, S. A., Schon, A., Goodman, B., Wang, Y., Yates, J., 3rd, Freire, E., Schroer, T. A. and Zheng, Y. (2013). Nudel/NudE and Lis1 promote dynein and dynactin interaction in the context of spindle morphogenesis. *Mol. Biol. Cell* **24**, 3522-3533.
Waters, A. M. and Beales, P. L. (2011). Ciliopathies: an expanding disease spectrum. *Pediatr. Nephrol.* **26**, 1039-1056.
Wickstead, B. and Gull, K. (2007). Dyneins across eukaryotes: a comparative genomic analysis. *Traffic* **8**, 1708-1721.
Zala, D., Hinckelmann, M. V., Yu, H., Lyra da Cunha, M. M., Liot, G., Cordelieres, F. P., Marco, S. and Saudou, F. (2013). Vesicular glycolysis provides on-board energy for fast axonal transport. *Cell* **152**, 479-491.
Zhou, T., Zimmerman, W., Liu, X. and Erikson, R. L. (2006). A mammalian NudC-like protein essential for dynein stability and cell viability. *Proc. Natl. Acad. Sci. USA* **103**, 9039-9044.

TABLE 1: PROTEOMIC ANALYSIS OF MGFP-WDR34 VERSUS MGFP IN STABLY-TRANSFECTED, SERUM-STARVED HTERT-RPE1 CELLS.

TABLE 1A: CYTOPLASMIC DYNEIN-2 SUBUNITS, NOT FOUND ASSOCIATED WITH DYNEIN-1

Accession	# AAs	MW [kDa]	Description	Score mGFP	Coverage mGFP	# PSM mGFP	# Peptides mGFP	Score mGFP-WDR34	Coverage mGFP-WDR34	# PSM mGFP-WDR34	# Peptides mGFP-WDR34	Annotation
Q96EX3	536	57.8	WD repeat-containing protein 34 GN=WDR34	137.93	44.59	31	16	3732.64	79.85	873	34	DYNEIN WDR34
Q8WVS4	1066	122.5	WD repeat-containing protein 60 GN=WDR60	n.d.	n.d.	n.d.	n.d.	329.54	37.24	89	33	DYNEIN WDR60
B0I1S0	4307	492.3	DYNC2H1 variant protein GN=DYNC2H1	n.d.	n.d.	n.d.	n.d.	37.31	2.48	10	10	DYNEIN HEAVY CHAIN 2
E5RJK4	72	7.9	Cytoplasmic dynein-2 light intermediate chain GN=DYNC2LI1	n.d.	n.d.	n.d.	n.d.	5.38	20.83	1	1	DYNEIN LIC3
Q8WW35	142	16.1	Tctex1 domain-containing protein 2 GN=TCTEX1D2	n.d.	n.d.	n.d.	n.d.	110.43	45.07	24	5	DYNEIN TCTEX1D2

n.d. = not detected

TABLE 1B: DYNEIN-1 LIGHT CHAINS ALSO FOUND ASSOCIATED WITH DYNEIN-2

Accession	# AAs	MW [kDa]	Description	Score mGFP	Coverage mGFP	# PSM mGFP	# Peptides mGFP	Score mGFP-WDR34	Coverage mGFP-WDR34	# PSM mGFP-WDR34	# Peptides mGFP-WDR34	Annotation
P63172	113	12.4	Dynein light chain Tctex-type 1 GN=DYNLT1	n.d.	n.d.	n.d.	n.d.	84.63	60.18	19	4	DYNEIN TCTEX1
P51808	116	13.1	Dynein light chain Tctex-type 3 GN=DYNLT3	n.d.	n.d.	n.d.	n.d.	7.97	23.28	3	2	DYNEIN TCTEX3
A4D1D1	297	32.5	Similar to dynein, cytoplasmic, light peptide; 8kD LC; dynein LC8; protein inhibitor of neuronal nitric oxide synthase GN=LOC392067	n.d.	n.d.	n.d.	n.d.	4.21	7.41	2	1	DYNEIN LC8
P63167	89	10.4	Dynein light chain 1, cytoplasmic OS=Homo sapiens GN=DYNLL1	23.71	64.04	7	5	405.41	64.04	109	6	DYNEIN LIGHT CHAIN 1
Q96FJ2	89	10.3	Dynein light chain 2, cytoplasmic OS=Homo sapiens GN=DYNLL2	19.29	25.84	5	3	255.84	65.17	81	6	DYNEIN LIGHT CHAIN 2
Q9NP97	96	10.9	Dynein light chain roadblock-type 1 OS=Homo sapiens GN=DYNLRB1	52.23	55.21	16	4	709.81	85.42	202	10	DYNEIN ROADBLOCK
Q8TF09	96	10.8	Dynein light chain roadblock-type 2 OS=Homo sapiens GN=DYNLRB2	19.08	16.67	6	2	170.55	33.33	54	3	DYNEIN ROADBLOCK 2

n.d. = not detected

TABLE 1C: DYNEIN-1 ACCESSORY FACTORS ALSO FOUND IN ASSOCIATION WITH DYNEIN-2

Accession	# AAs	MW [kDa]	Description	Score mGFP	Coverage mGFP	# PSM mGFP	# Peptides mGFP	Score mGFP-WDR34	Coverage mGFP-WDR34	# PSM mGFP-WDR34	# Peptides mGFP-WDR34	Annotation
B0FTY2	361	40.8	NudC-like protein OS=Homo sapiens GN=NUDCD3	n.d.	n.d.	n.d.	n.d.	7.77	5.54	3	2	NUDCD3
Q9Y266	331	38.2	Nuclear migration protein NudC OS=Homo sapiens GN=NUDC	7.33	3.32	2	1	27.18	10.57	7	3	NUDC

n.d. = not detected

TABLE 1D: DYNEIN-1 ACCESSORY FACTORS THAT WERE NOT FOUND IN ASSOCIATION WITH DYNEIN-2

Accession	# AAs	MW [kDa]	Description	Score mGFP	Coverage mGFP	# PSM mGFP	# Peptides mGFP	Score mGFP-WDR34	Coverage mGFP-WDR34	# PSM mGFP-WDR34	# Peptides mGFP-WDR34	Annotation
G5E9H4	1139	126.7	Dynactin 1 (P150, glued homolog, Drosophila), isoform CRA_a OS=Homo sapiens GN=DCTN1	2.70	1.14	1	1	10.04	1.05	1	1	DYNACTIN
H0YIC1	228	25.4	Bicaudal D-related protein 1 (Fragment) OS=Homo sapiens GN=CCDC64	n.d.	n.d.	n.d.	n.d.	2.43	4.39	1	1	BICAUDAL D1
B4DWL0	270	30.9	Bicaudal D-related protein 1 OS=Homo sapiens GN=CCDC64	19.73	5.19	2	1	n.d.	n.d.	n.d.	n.d.	BICAUDAL D RELATED PROTEIN 1
I3L2U8	345	38.9	Platelet-activating factor acetylhydrolase IB subunit alpha OS=Homo sapiens GN=PAFAH1B1	6.44	9.28	2	2	n.d.	n.d.	n.d.	n.d.	LIS1

n.d. = not detected

Figure 1

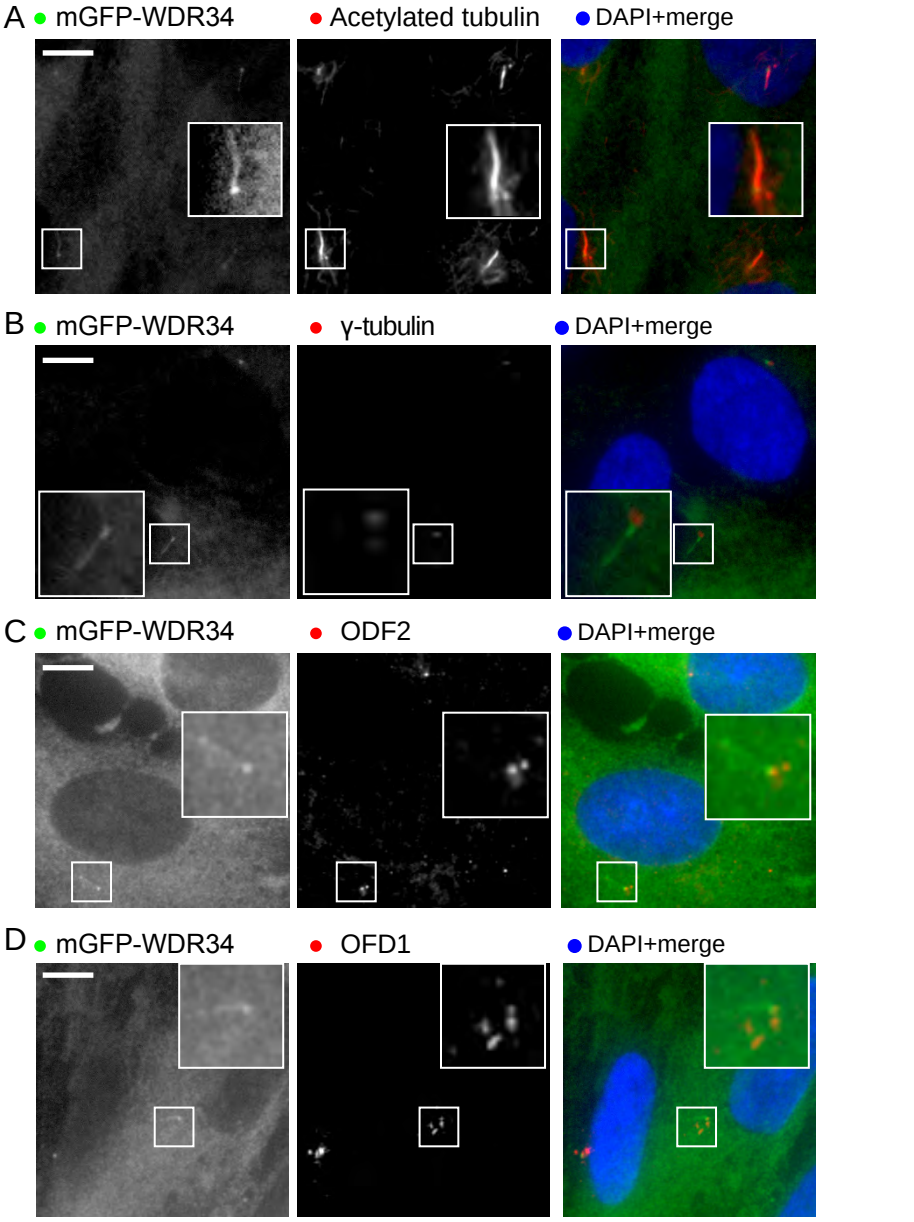
A
mGFP-WDR34
Acetylated tubulin
DAPI+merge
B
mGFP-WDR34
γ-tubulin
DAPI+merge
C
mGFP-WDR34
ODF2
DAPI+merge
D
mGFP-WDR34
OFD1
DAPI+merge

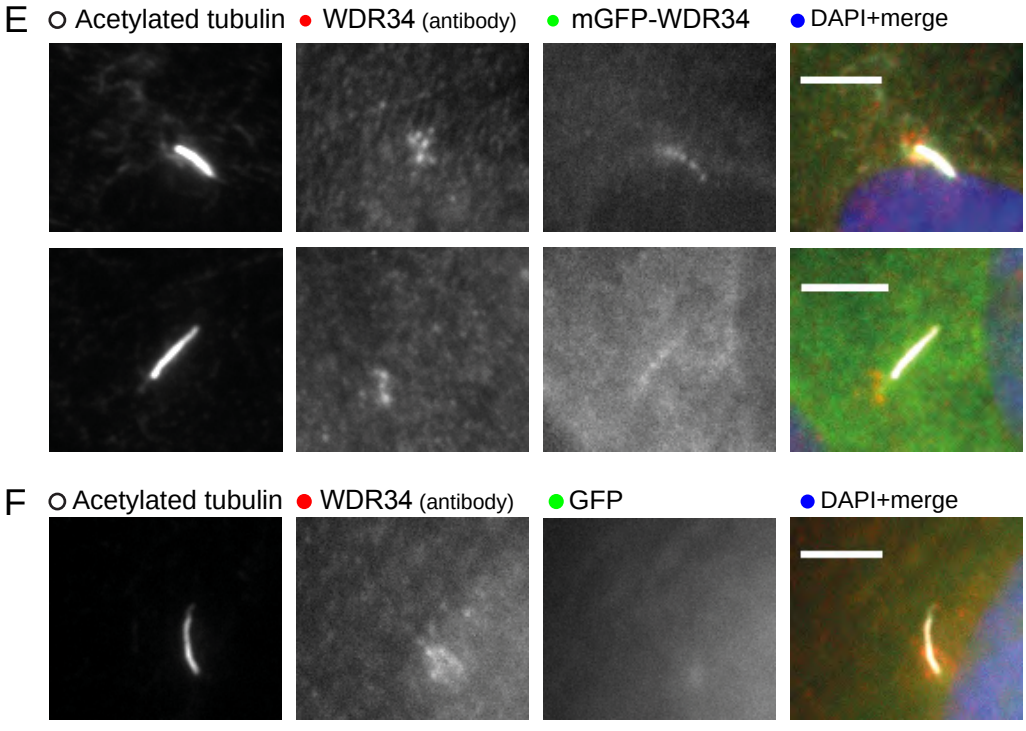
E
Acetylated tubulin
WDR34 (antibody)
mGFP-WDR34
DAPI+merge
F
Acetylated tubulin
WDR34 (antibody)
GFP
DAPI+merge

Figure 2

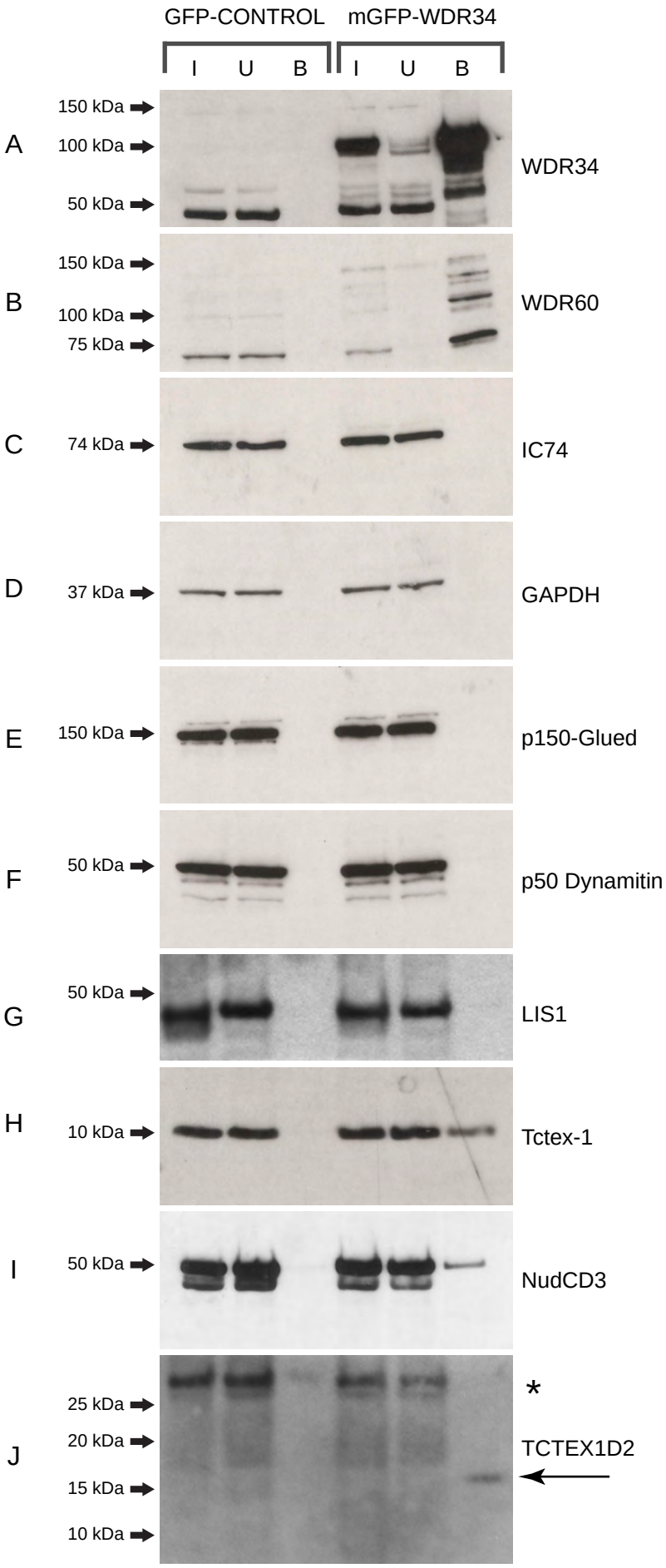
GFP-CONTROL
mGFP-WDR34
I
U
B
I
U
B
A
150 kDa
100 kDa
50 kDa
WDR34
B
150 kDa
100 kDa
75 kDa
WDR60
C
74 kDa
IC74
D
37 kDa
GAPDH
E
150 kDa
p150-Glued
F
50 kDa
p50 Dynamitin
G
50 kDa
LIS1
H
10 kDa
Tctex-1
I
50 kDa
NudCD3
J
25 kDa
20 kDa
15 kDa
10 kDa
*
TCTEX1D2

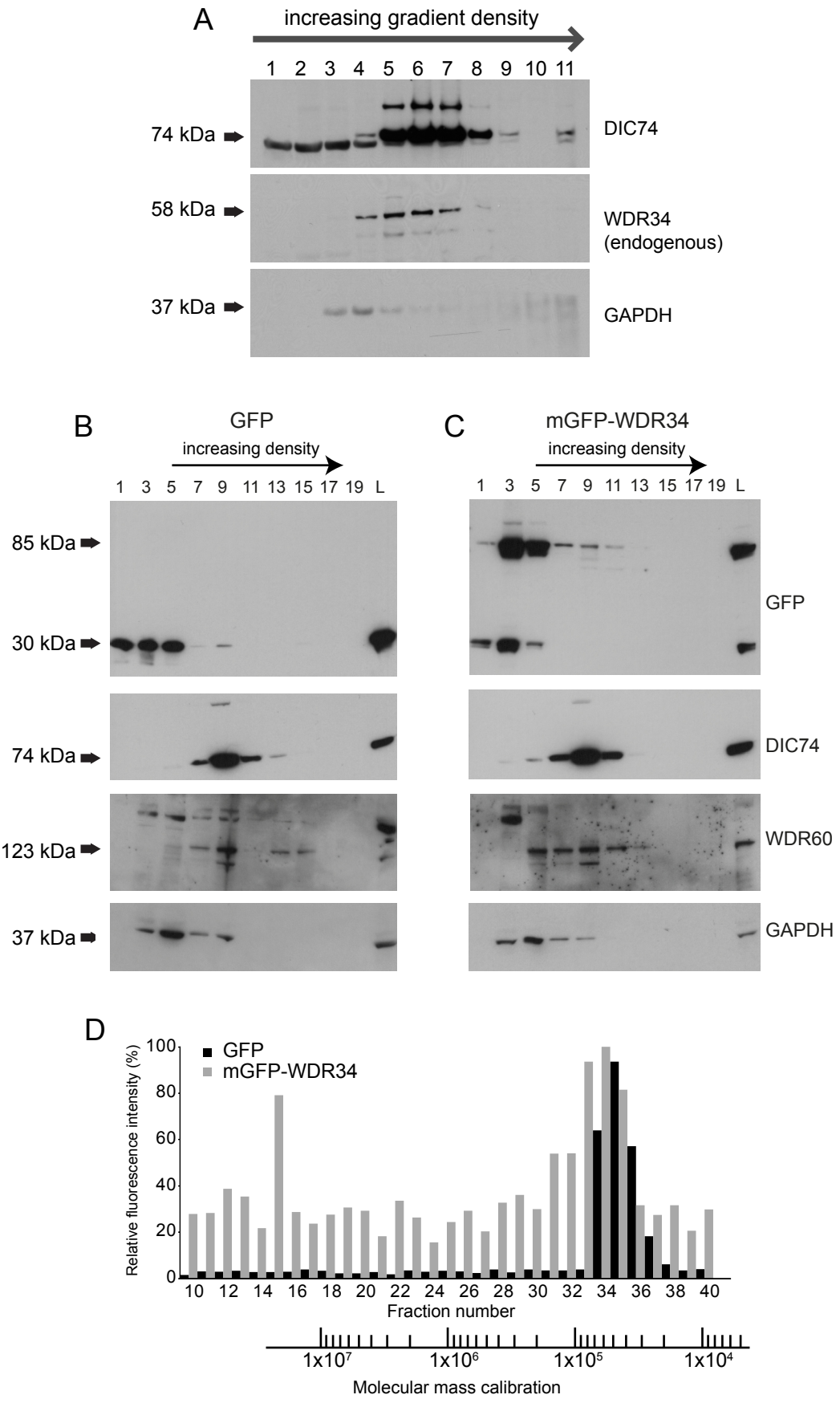
A
increasing gradient density
1 2 3 4 5 6 7 8 9 10 11
74 kDa
DIC74
58 kDa
WDR34
(endogenous)
37 kDa
GAPDH
B
GFP
increasing density
1 3 5 7 9 11 13 15 17 19 L
85 kDa
30 kDa
74 kDa
123 kDa
37 kDa
C
mGFP-WDR34
increasing density
1 3 5 7 9 11 13 15 17 19 L
GFP
DIC74
WDR60
GAPDH
D
GFP
mGFP-WDR34
Relative fluorescence intensity (%)
100
80
60
40
20
0
10 12 14 16 18 20 22 24 26 28 30 32 34 36 38 40
Fraction number
1x10^7
1x10^6
1x10^5
1x10^4
Molecular mass calibration

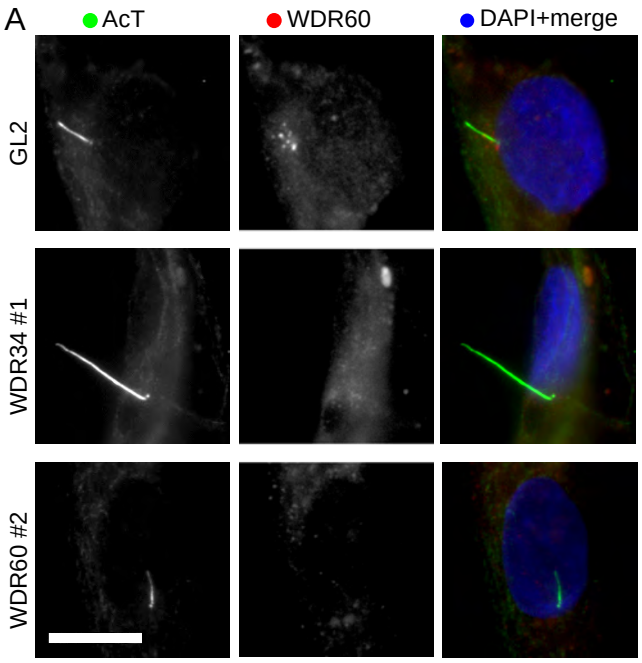
A
AcT
WDR60
DAPI+merge
GL2
WDR34 #1
WDR60 #2

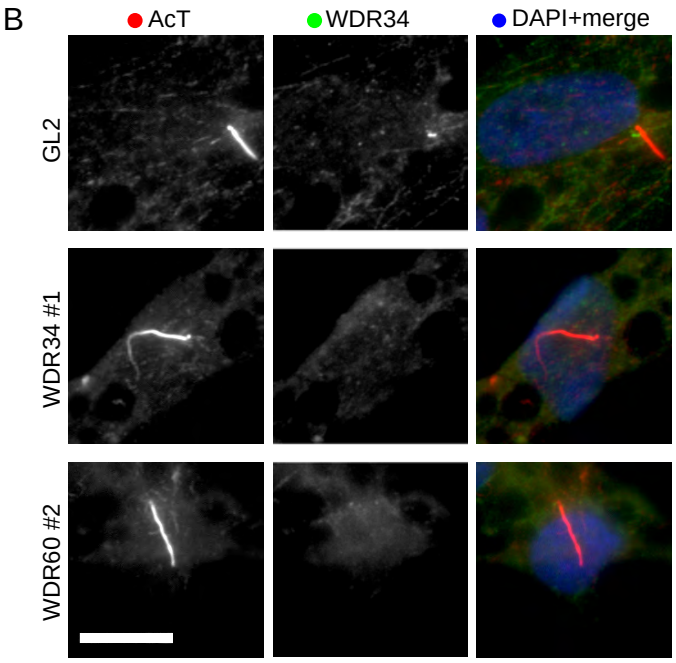
B
AcT
WDR34
DAPI+merge
GL2
WDR34 #1
WDR60 #2

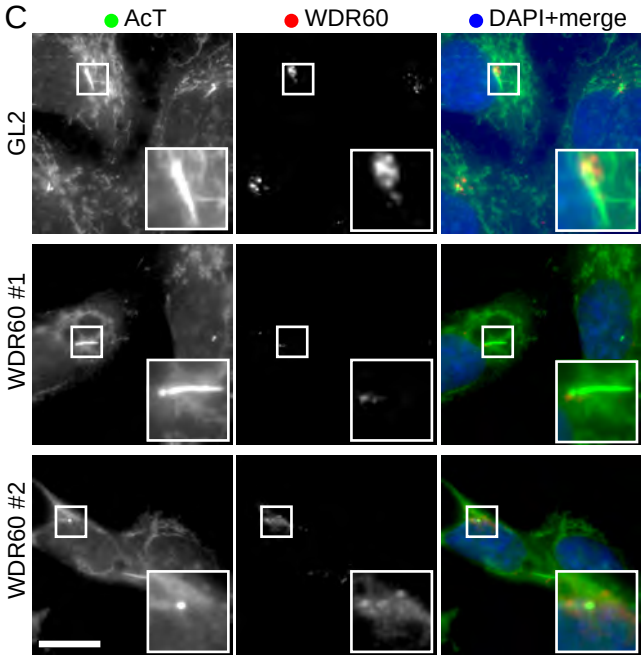
C
AcT
WDR60
DAPI+merge
GL2
WDR60 #1
WDR60 #2

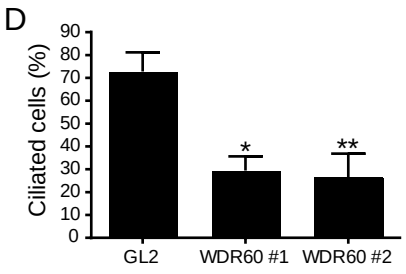
D
Ciliated cells (%)
GL2
WDR60 #1
WDR60 #2

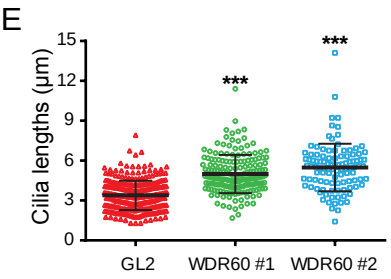
E
Cilia lengths (μm)
GL2
WDR60 #1
WDR60 #2

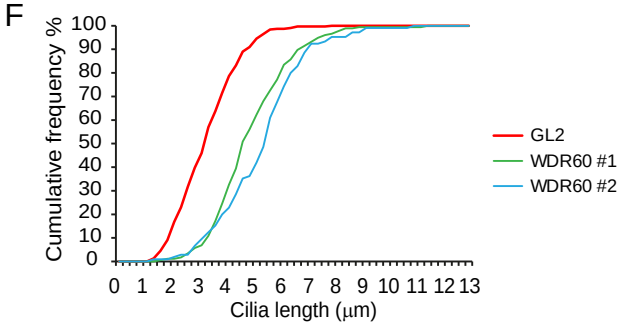
F
Cumulative frequency %
Cilia length (μm)
GL2
WDR60 #1
WDR60 #2

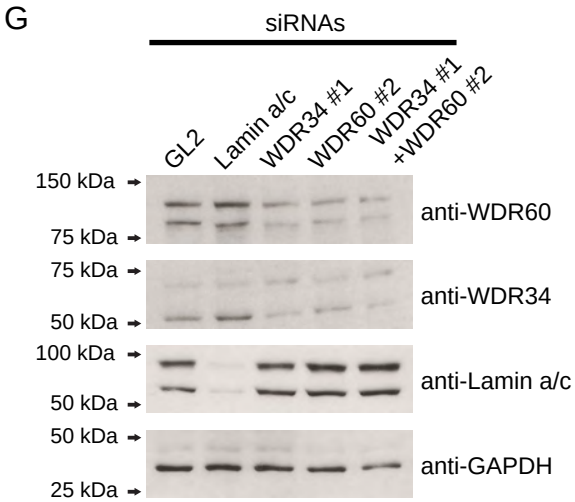
G
siRNAs
GL2
Lamin a/c
WDR34 #1
WDR60 #2
WDR34 #1 +WDR60 #2
150 kDa
75 kDa
anti-WDR60
75 kDa
50 kDa
anti-WDR34
100 kDa
50 kDa
anti-Lamin a/c
50 kDa
25 kDa
anti-GAPDH

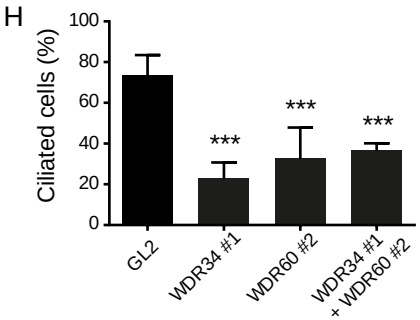
H
Ciliated cells (%)
GL2
WDR34 #1
WDR60 #2
WDR34 #1 + WDR60 #2

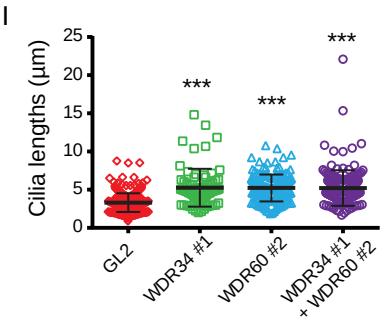
I
Cilia lengths (μm)
GL2
WDR34 #1
WDR60 #2
WDR34 #1 + WDR60 #2

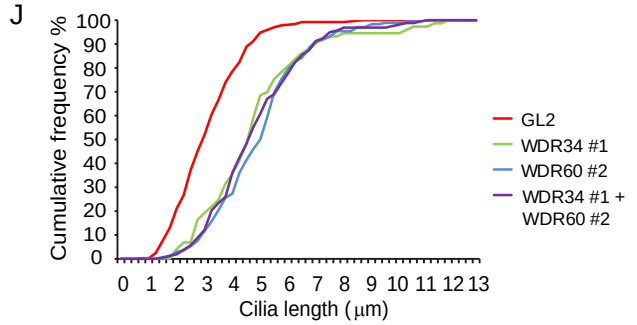
J
Cumulative frequency %
Cilia length (μm)
GL2
WDR34 #1
WDR60 #2
WDR34 #1 + WDR60 #2

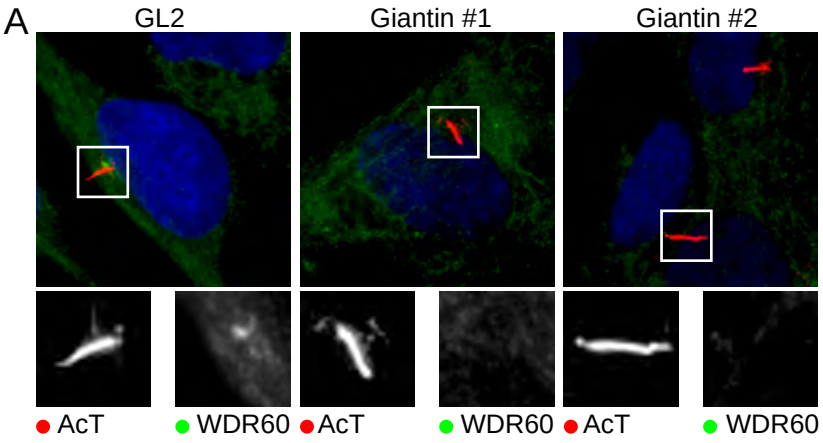
A
GL2
Giantin #1
Giantin #2
AcT
WDR60
AcT
WDR60
AcT
WDR60

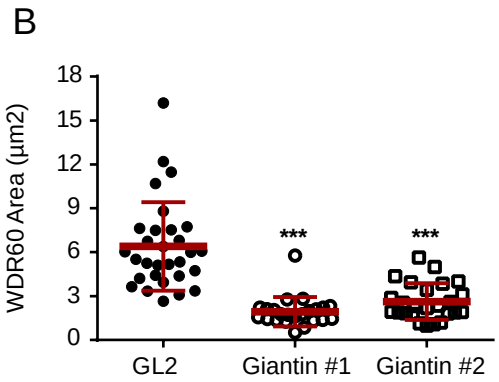
B
WDR60 Area (µm2)
18
15
12
9
6
3
0
***
***
GL2
Giantin #1
Giantin #2

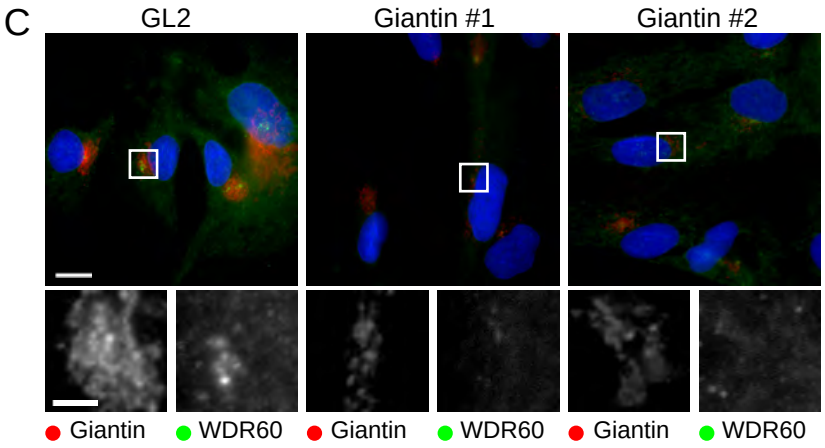
C
GL2
Giantin #1
Giantin #2
Giantin
WDR60
Giantin
WDR60
Giantin
WDR60

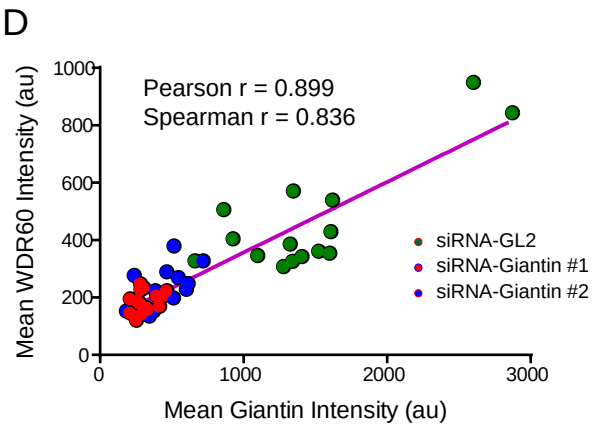
D
Mean WDR60 Intensity (au)
1000
800
600
400
200
0
Pearson r = 0.899
Spearman r = 0.836
siRNA-GL2
siRNA-Giantin #1
siRNA-Giantin #2
0
1000
2000
3000
Mean Giantin Intensity (au)

Figure 6

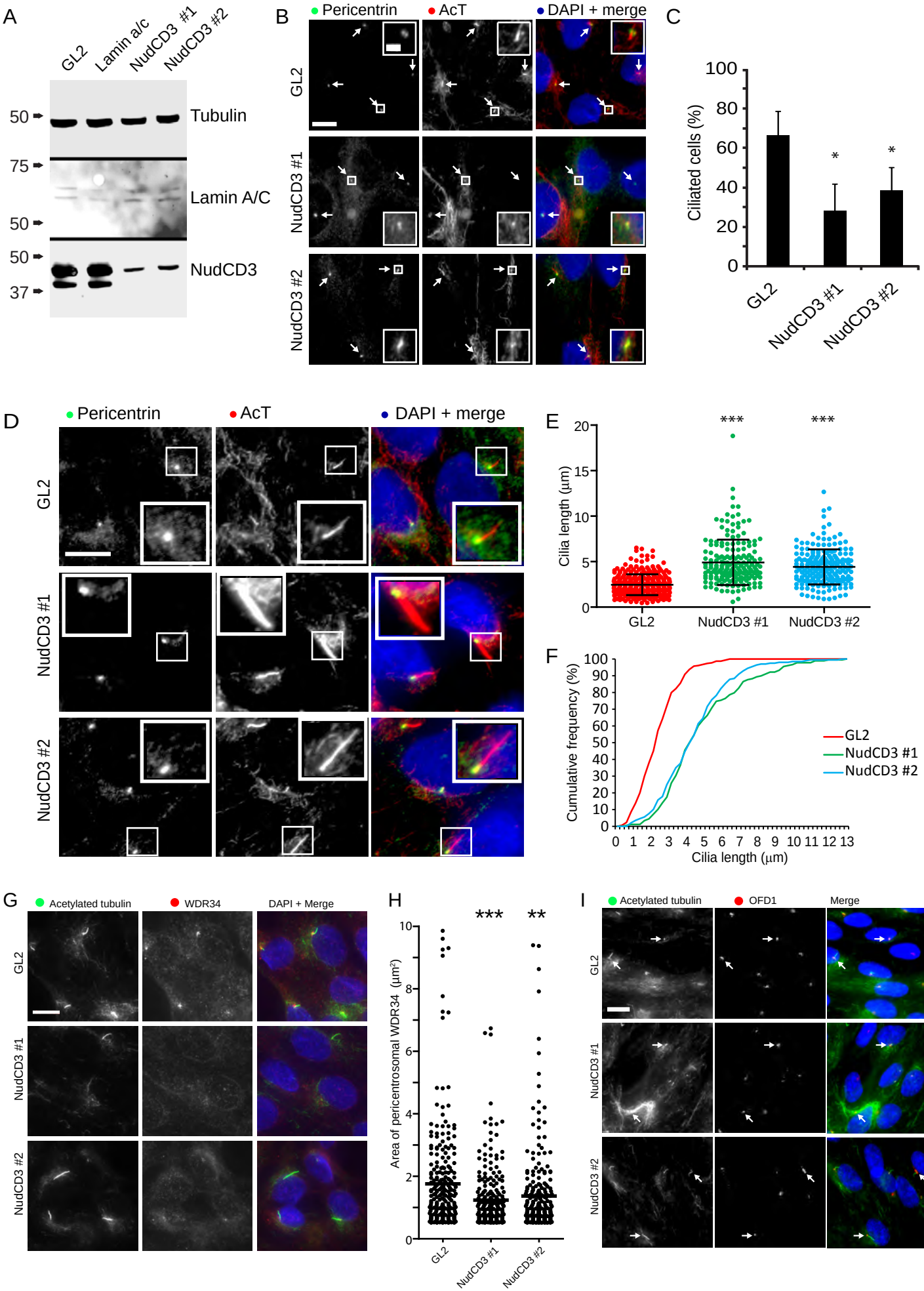
A
GL2
Lamin a/c
NudCD3 #1
NudCD3 #2
50
75
50
50
37
Tubulin
Lamin A/C
NudCD3
B
Pericentrin
AcT
DAPI + merge
GL2
NudCD3 #1
NudCD3 #2
C
Ciliated cells (%)
100
80
60
40
20
0
*
*
GL2
NudCD3 #1
NudCD3 #2
D
Pericentrin
AcT
DAPI + merge
GL2
NudCD3 #1
NudCD3 #2
E
Cilia length (µm)
20
15
10
5
0
***
***
GL2
NudCD3 #1
NudCD3 #2
F
Cumulative frequency (%)
100
90
80
70
60
50
40
30
20
10
0
0 1 2 3 4 5 6 7 8 9 10 11 12 13
Cilia length (µm)
GL2
NudCD3 #1
NudCD3 #2
G
Acetylated tubulin
WDR34
DAPI + Merge
GL2
NudCD3 #1
NudCD3 #2
H
Area of pericentrosomal WDR34 (µm²)
10
8
6
4
2
0
***
**
GL2
NudCD3 #1
NudCD3 #2
I
Acetylated tubulin
OFD1
Merge
GL2
NudCD3 #1
NudCD3 #2

Figure 7

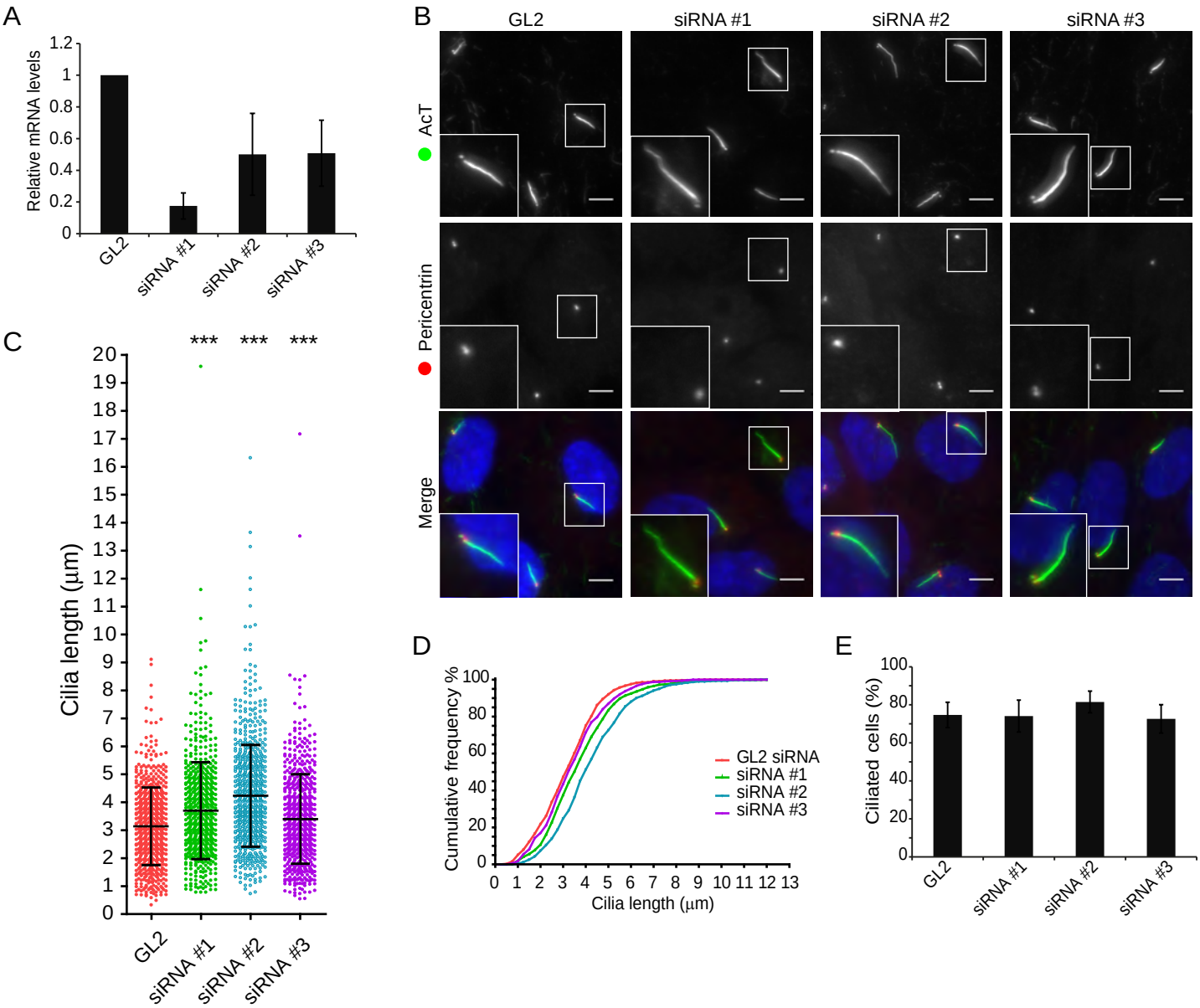
A
Relative mRNA levels
1.2
1
0.8
0.6
0.4
0.2
0
GL2
siRNA #1
siRNA #2
siRNA #3
B
GL2
siRNA #1
siRNA #2
siRNA #3
AcT
Pericentrin
Merge
C
***
***
***
Cilia length (μm)
20
19
18
17
16
15
14
13
12
11
10
9
8
7
6
5
4
3
2
1
0
GL2
siRNA #1
siRNA #2
siRNA #3
D
Cumulative frequency %
100
80
60
40
20
0
0 1 2 3 4 5 6 7 8 9 10 11 12 13
Cilia length (μm)
GL2 siRNA
siRNA #1
siRNA #2
siRNA #3
E
Ciliated cells (%)
100
80
60
40
20
0
GL2
siRNA #1
siRNA #2
siRNA #3

Figure 8

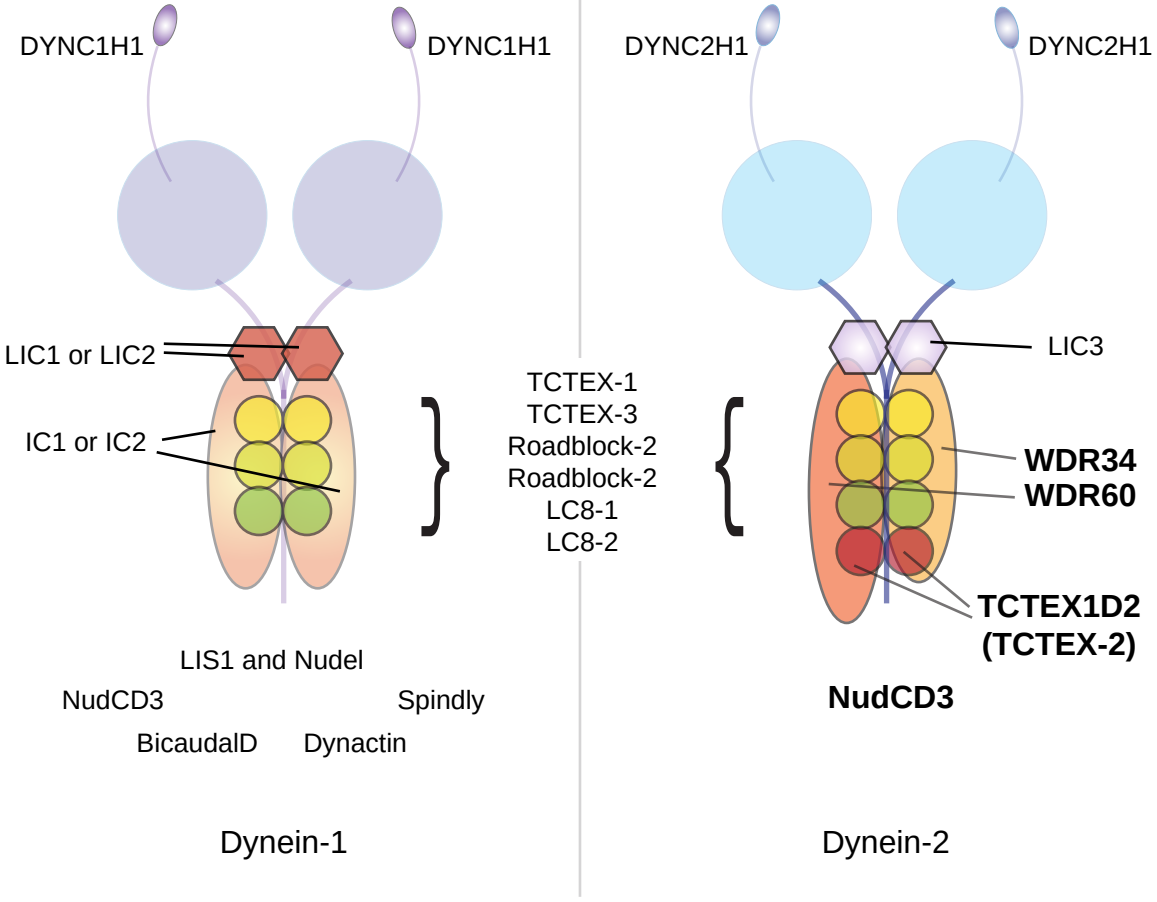
DYNC1H1
DYNC1H1
LIC1 or LIC2
IC1 or IC2
LIS1 and Nudel
NudCD3
Spindly
BicaudalD
Dynactin
Dynein-1
TCTEX-1
TCTEX-3
Roadblock-2
Roadblock-2
LC8-1
LC8-2
DYNC2H1
DYNC2H1
LIC3
WDR34
WDR60
TCTEX1D2
(TCTEX-2)
NudCD3
Dynein-2